Symmetric vs. Asymmetric Linear M-X-M Linkages in Molecules, Polymers, and Extended Networks

Ralph A. Wheeler,[†] Myung-Hwan Whangbo,[‡] Timothy Hughbanks,[⊥] Roald Hoffmann,*[†] Jeremy K. Burdett,[⊥] and Thomas A. Albright[∥]

Contribution from the Department of Chemistry and Materials Science Center, Cornell University, Ithaca, New York 14853, the Department of Chemistry, North Carolina State University, Raleigh, North Carolina 27695-8204, the Department of Chemistry, the University of Chicago, Chicago, Illinois 60637, and the Department of Chemistry, the University of Houston, Houston, Texas 77004. *Received August 6, 1985*

Abstract: Linear M-X-M linkages in which X is a nitride, oxide, or halide commonly occur in dimers, square tetramers, one-dimensional polymers, and extended three-dimensional solids. For low d electron counts a second-order Jahn-Teller mixing of metal d_π and X p_π orbitals favors asymmetric M-X···M bridges. M-X σ bonding works against the distortion. Going to higher d electron counts also favors the symmetrical bridge by filling M-X π^* levels. For the cyclic $[ML_4X]_4$ tetramer and $^1_\infty[ML_4X]$ chain, d electron counts greater than two favor a symmetric bridge; for perovskites, d^n metals with $n \geq 1$ are calculated to be symmetric. The extent of M-X bond length alternation can also be decreased by increasing the electronegativity difference between M and X to widen the HOMO-LUMO gap.

Vertex-sharing polyhedra abound in solid-state and molecular transition-metal chemistry. Ever since Taube's classic work with $Cr(OH_2)_6^{2+}$, studies of inner-sphere electron-transfer reactions have focused on an intermediate with two octahedrally coordinated metal atoms sharing a common bridging ligand.[1] Similarly, some of the oldest, most extensively studied metallic compounds are the tungsten bronzes.[2] The cubic modification of the tungsten bronzes adopts the simple cubic array of corner linked WO_3 octahedra shown in **1**. The octahedra are arranged to form linear W-O-W bridges and cube centers are randomly occupied by metal

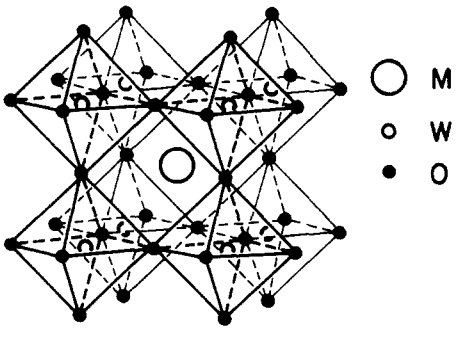

1

counterions to give the stoichiometry M_xWO_3. A vast number of other transition-metal oxides, halides, and oxyhalides adopt this same cubic perovskite structure, as well as its tetragonal, orthorhombic and hexagonal cousins.[3] Interesting physical properties include not only metallic but also ferroelectric and magnetic behavior.[4] The ferroelectric properties of perovskites are correlated with their structural features.

Intermediate between the simple dimers and infinite three-dimensional arrays of corner linked octahedra are a number of structurally similar oligomers, one-dimensional polymers, and two-dimensional sheets. These are exemplified by the tetramer $[MoNCl_3]_4$, **2**,[5,6a(i)] the polymer $ReNCl_4$, **3**,[5,7] and the sheet of octahedral chains cross-linked by corner-sharing tetrahedra of α-$VOPO_4$, **4**.[8a] These molecules, a natural link between simple monomer complexes and extended three-dimensional systems, are the subject of this paper. An overview of the structural features

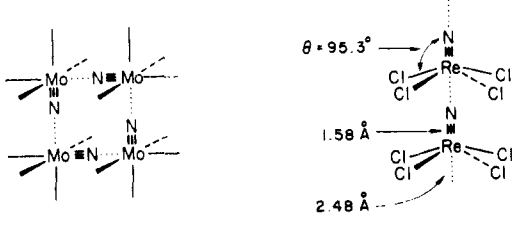

2 **3**

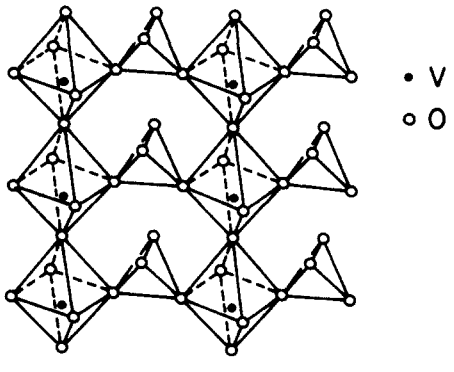

4

of these oligomers and polymers will show that they have in common a distorted coordination sphere around the metal. In

[†] Cornell University.
[‡] North Carolina State University.
[⊥] University of Chicago.
[∥] University of Houston.

(1) (a) (i) Taube, H. *Chem. Rev.* **1952**, *50*, 69. (ii) Taube, H.; Myers, H.; Rich, R. L. *J. Am. Chem. Soc.* **1953**, *75*, 4118. (iii) Taube, H.; Myers, H. *J. Am. Chem. Soc.* **1954**, *76*, 2103. (b) For a recent review see: Haim, A. *Prog. Inorg. Chem.* **1983**, *30*, 273.

(2) (a) Wohler, F. *Pogg. Ann.* **1824**, *2*, 350. (b) (i) Goodenough, J. B. *Prog. Solid State Chem.* **1971**, *5*, 313. (ii) Hagenmuller, P. *Ibid.* **1971**, *5*, 175.

(3) (a) Müller, O.; Roy, R. "The Major Ternary Structural Families"; Springer-Verlag: Berlin, 1974; p 174 ff. (b) Galasso, F. S. "Structure Properties, and Preparation of Perovskite-Type Compounds"; Pergamon Press: Oxford, 1969. (c) Triclinic WO_3: Diehl, R.; Brandt, G.; Salje, E. *Acta Crystallogr.* **1978**, *B34*, 1105. (d) Monoclinic WO_3: Loopstra, B. O.; Rietveld, H. M. *Acta Crystallogr.* **1969**, *B25*, 1420. (e) Orthorhombic WO_3: Salje, E. *Acta Crystallogr.* **1977**, *B33*, 574. (f) Na_xWO_3: Straumanis, M. E. *J. Am. Chem. Soc.* **1949**, *71*, 679. (g) Tetragonal $BaTiO_3$: Frazer, B. C.; Danner, H. R.; Pepinsky, R. *Phys. Rev.* **1955**, *100*, 745. (h) $KNbO_3$: Katz, L.; Megaw, H. D. *Acta Crystallogr.* **1967**, *22*, 639. (i) $Sr_{0.5+x}NbO_3$: Ridgley, D.; Ward, R. *J. Am. Chem. Soc.* **1955**, *77*, 6132. (j) $Ba_{0.5+x}NbO_3$: Kreiser, R. R.; Ward, R. *J. Solid State Chem.* **1970**, *1*, 368. (k) $K_{0.92}MoO_3$: Bither, T. A.; Gillson, J. L.; Young, H. S. *Inorg. Chem.* **1966**, *5*, 1559.

0002-7863/86/1508-2222$01.50/0 © 1986 American Chemical Society

each case the distortion can be understood in terms of a simple symmetry argument, buttressed by extended Hückel molecular orbital calculations[9] (parameters specified in Appendix). An understanding of the bonding also provides some insight into the properties and reactivity of these compounds.

In the nitride tetramers,[6] structural distortions can be analyzed in terms of octahedral tilting combined with changing bond lengths and angles within octahedra,[10] but we focus upon the characteristic bond length alternation show in **2**. Several molecules with this square-planar metal–nitrogen core and alternating M–N bond lengths are known.[6] Each has a short M≡N bond in the range 1.64–1.69 Å and a long M···N bonding contact, 2.11–2.17 Å. The octahedral coordination sphere for each metal atom consists of the two bridging nitrogen and three chloride ligands, with a sixth ligand weakly bound trans to the short metal–nitrogen bond. The sixth ligand is usually a solvent molecule, but in $[MoNCl_3]_4$ and $[WNCl_3{\cdot}0.5HN_3]_4$ the tetrameric rings orient so that the sixth coordination site of each metal is occupied by a chloride ligand from a neighboring ring. If we assign the nitride a 3- formal oxidation state, all metals are 6+, d^0. It is also reported that the d^1 compound $[ReNCl_3{\cdot}OPCl_3]_4$ is isotypic with $[WNCl_3{\cdot}OPCl_3]_4{\cdot}2POCl_3$.[6b] Another molecule, $[MoN(S_2P(OR)_2)_2]_4$, contains the square metal–nitrogen core, **2**, but with all Mo–N bond lengths equal.[6c] We will argue later that in this case the unique ligand set governs Mo–N bond lengths. The majority of tetramers composed of cis corner linked octahedra show M–N bond length alternation as indicated in **2**.

Like the tetramers, nitrido-bridged polymers show the alternating metal–nitrogen bond lengths represented in **3**.[7] That example, $ReNCl_4$, has a structure typical of those built from trans corner-linked octahedra. In addition to the Re–N bond length alternation, the chloride ligands bend away from the short Re–N bond, much as they would bend away from the apex of a square-pyramidal molecule. This distortion suggests an alternate way to view the nitrido-bridged polymers. They are composed of C_{4v} $ReNCl_4$ fragments linked to neighboring molecules in the chain by their apical nitrogen atoms.

The asymmetry seen in the $ReNCl_4$ polymer also appears in other corner-linked polyhedral chains. Recently a linear nitrido polymer built up from corner-linked trigonal bipyramids, **5**, $(t\text{-BuO})_3WN$, has been synthesized[11a] and its structure determined.[11b,d] The bond length alternation and pyramidalization about the metal suggest that the crystal and electronic structure of polymer $(t\text{-BuO})_3W{\equiv}N$ can be built up from molecular $(RO)_3W{\equiv}N$ units.

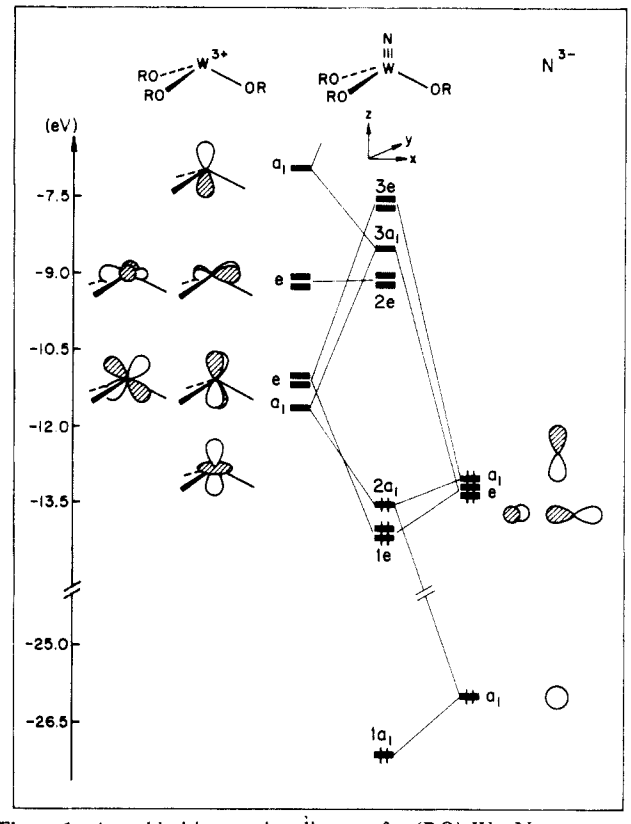

Figure 1. An orbital interaction diagram for $(RO)_3W{\equiv}N$.

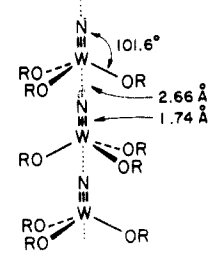

5

Oxo-bridged chains showing similar distortions can be identified in layered compounds of the type $MOXO_4$ (M = V with X = P, S, Mo; M = Nb, Ta, Mo with X = P). **4** shows the MO_6 octahedral chains in α-$VOPO_4$ cross-linked by corner-sharing XO_4 tetrahedra. The observed short, long M–O distance pairs range from 1.786, 2.215 in $TaOPO_4$[8e] to 1.580, 2.857 in α-$VOPO_4$.[8a]

Let us begin our analysis with an examination of a typical monomeric nitride, $L_3W{\equiv}N$. From it we will build geometrically and electronically the oligomer and polymer structures.

The $(RO)_3W{\equiv}N$ Monomer and Dimer

The electronic structure of $(RO)_3W{\equiv}N$ is most easily constructed by interacting a $(RO)_3W^{3+}$ fragment with a N^{3-} atom. This is done in Figure 1. On the left side of this figure are the

(4) (a) Goodenough, J. B.; Longo, J. M. In *LANDOLT-BORNSTEIN TABELLEN*, New Series III/4a; Hellwege, K. H.., Hellwege, A. M.., Eds.; Springer-Verlag: Berlin, 1970; p 162. (b) Abe, R.; Furuhata, Y.; Ikeda, T.; Makita, Y.; Marutake, M.; Nakamura, E.; Nomura, S.; Sawaguchi, E.; Shiozaki, Y.; Toyoda, K. In *LANDOLT-BORNSTEIN TABELLEN*, New Series III/3; Hellwege, K. H., Hellwege, A. M., Eds.; Springer-Verlag: Berlin, 1969; p 37. (c) Jona, F.; Shirane, G. "Ferroelectric Crystals"; MacMillan: New York, 1962; Chapters IV and V.

(5) For a review of nitrido compounds, see: (a) Dehnicke, K.; Strähle, J. *Angew. Chem.* **1981**, *93*, 451; *Angew. Chem., Int. Ed. Engl.* **1981**, *20*, 413. (b) Griffith, W. P. *Coord. Chem. Rev.* **1972**, *8*, 369.

(6) (a) (i) Strähle, J. *Z. Anorg. Allg. Chem.* **1970**, *375*, 238; **1971**, *380*, 96. (ii) Müller, U.; Kujanek, R.; Dehnicke, K. *Z. Anorg. Allg. Chem.* **1982**, *495*, 127. (iii) Strähle, J.; Weiher, U.; Dehnicke, K. *Z. Naturforsch.* **1978**, *B33*, 1347. (iv) Musterle, W.; Strähle, J.; Liebelt, W.; Dehnicke, K. *Z. Naturforsch.* **1979**, *B34*, 942. (v) Walker, I.; Strähle, J.; Ruschke, P.; Dehnicke, K. *Z. Anorg. Allg. Chem.* **1982**, *487*, 26. (b) Liese, W.; Dehnicke, K.; Walker, I.; Strähle, J. *Z. Naturforsch.* **1980**, *B35*, 776. (c) Noble, M. E.; Folting, K.; Huffman, J. C.; Wentworth, R. A. D. *Inorg. Chem.* **1982**, *21*, 3772.

(7) (a) Liese, W.; Dehnicke, K.; Walker, I.; Strähle, J. *Z. Naturforsch.* **1979**, *B34*, 693. (b) Davies, W. O.; Johnson, N. P.; Johnson, P.; Graham, A. J. *J. Chem. Soc., Chem. Commun.* **1969**, 736.

(8) (a) Jordan, B.; Calvo, C. *Can. J. Chem.* **1973**, *51*, 2621. (b) Longo, J. M.; Arnott, R. J. *J. Solid State Chem.* **1970**, *1*, 394. (c) Eick, H. A.; Kihlborg, L. *Acta Chem. Scand.* **1966**, *20*, 722. (d) Longo, J. M.; Kierkegaard, P. *Acta Chem. Scand.* **1966**, *20*, 72. (e) Longo, J. M.; Pierce, J. W.; Kafalas, J. A. *Mater. Res. Bull.* **1971**, *6*, 1157. (f) Kierkegaard, P.; Westerlund, M. *Acta Chem. Scand.* **1964**, *18*, 2217.

(9) (a) Hoffmann, R.; Lipscomb, W. N. *J. Chem. Phys.* **1962**, *36*, 2179, 3489; **1962**, *37*, 2872. (b) Hoffmann, R. *Ibid.* **1963**, *39*, 1397.

(10) (a) Glazer. A. M. *Acta Crystallogr.* **1975**, *A31*, 756. (b) Glazer, A. M. *Acta Crystallogr.* **1972**, *B28*, 3384.

(11) (a) Schrock, R. R.; Listemann, M. L.; Sturgeoff, L. G. *J. Am. Chem. Soc.* **1982**, *104*, 4291. (b) Chisholm, M. H.; Hoffman, D. M.; Huffman, J. C. *Inorg. Chem.* **1983**, *22*, 2903. (c) Cotton, F. A.; Schwotzer, W.; Shamshoum, E. S. *Organometallics* **1984**, *3*, 1770. (d) The molybdenum analogue $(t\text{-BuO})_3Mo{\equiv}N$ has recently been made: Chan, D. M.-T.; Chisholm, M. H.; Folting, K.; Huffman, J. C.; Marchant, N. S., private communication. In that complex the MoN distances in the one-dimensional chain are 1.66 and 2.86 Å.

important valence orbitals of the $(RO)_3W^{3+}$ fragment. This fragment is not distorted much from planarity (the N–W–O angles are 101.6°) and therefore the valence orbitals are very close to what one would expect for a D_{3h} ML_3 complex.[12] At high energy is a primarily metal z orbital of a_1 symmetry followed by an e set of $x^2 - y^2$ and xy character. Metal x and y also mix into it in a bonding way with respect to the σ hybrids of the alkoxide ligands. As noted previously[11b] the W–O distances are very short, which implies substantial π-donation from alkoxide lone pairs to the metal. One set of lone pairs does indeed overlap well with the $x^2 - y^2/xy$ set which keeps this latter fragment orbital set at high energy. At lower energy is an e set of predominately metal xz and yz character and z^2, which has a_1 symmetry. Normally z^2 is expected to lie above the xz/yz set when there are σ-donor ligands around the metal. However, strong π bonding from the alkoxide lone pairs inverts this orbital sequence.

The atomic x and y orbitals on nitrogen interact with the xz/yz set to produce a bonding molecular orbital, labeled 1e in Figure 1, and an antibonding counterpart, 3e. The 1e set is filled and concentrated on the more electronegative nitrogen atom. There is another molecular orbital at lower energy, concentrated on the oxygen atoms, which is π bonding between the metal and oxygen atoms. Returning to Figure 1, the $x^2 - y^2/xy$ set does not overlap to an appreciable extent with the nitrogen atomic orbitals because of its δ symmetry. Consequently metal $x^2 - y^2/xy$ remains nonbonding.

Metal z and z^2 along with nitrogen s and z overlap with each other to produce four molecular orbitals of a_1 symmetry. The three lowest molecular levels are shown in Figure 1. $1a_1$ consists of primarily nitrogen s mixed in a bonding way to metal z^2 and z. The $2a_1$ orbital is concentrated on nitrogen z, bonding to metal z^2, **6**. Furthermore, some nitrogen s character is mixed in second order in a way which is antibonding to z^2. This hybridizes the orbital at nitrogen away from the metal, as shown in **7**. The filled 1e and $1a_1$ molecular orbitals correspond to the π and σ bonds between tungsten and nitrogen. The $2a_1$ level, **7**, can then be

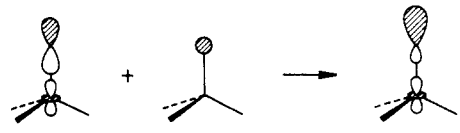

6 **7, $2a_1$**

identified with the filled lone pair at the nitrogen and is predicted to be the HOMO in the monomer. Besides 2e and 3e there is another low-lying empty orbital, labeled $3a_1$ in Figure 1. It is predominantly metal z^2 in character, mixed in an antibonding way to nitrogen z, **8**. What keeps $3a_1$ at relatively low energy is that metal z mixes into **8** in a way which is bonding to nitrogen z. As

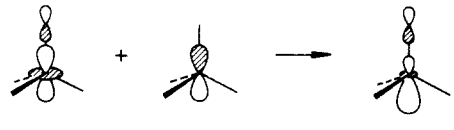

8 **9**

illustrated in **9** this hybridizes the orbital at the metal in a direction away from nitrogen. Plots of the filled $2a_1$ and empty $3a_1$ orbitals are presented in Figure 2, a and b, respectively. Thus, $(RO)_3W{\equiv}N$ contains a donor hybrid orbital of axial or σ symmetry concentrated at nitrogen and a low-lying acceptor orbital of the same symmetry localized on the tungsten atom. It is then easy to see why $(t\text{-BuO})_3W{\equiv}N$ assembles itself into the linear chain polymer shown in **5**. Stabilization of a $(RO)_3W{\equiv}C{-}R'$ complex will also be achieved by interaction of a low-lying acceptor analogous to $3a_1$ with a lone pair on an alkoxide ligand. Two

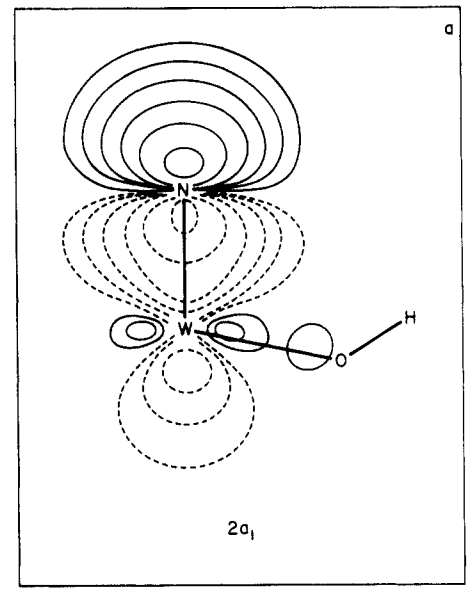

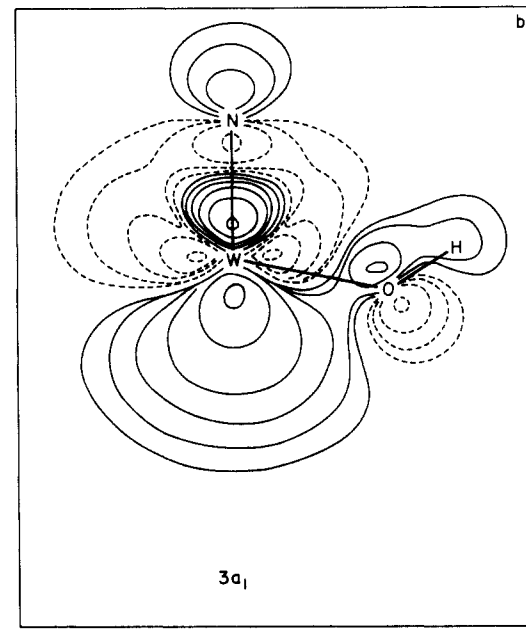

Figure 2. Plots of the filled $2a_1$ and empty $3a_1$ orbitals of $(RO)_3W{\equiv}N$. Values of the contours are ±0.4, ±0.2, ±0.1, ±0.05, ±0.025, and ±0.012.

examples are $(t\text{-BuO})_3W{\equiv}CMe_3$[11b] and $[t\text{-BuO})_3W{\equiv}C\text{-}NMe_2]_2$.[13] The monomeric $(t\text{-BuO})_3W{\equiv}CPh$,[11c] on the other hand, shows just how weak this interaction must be.

Aside from $3a_1$, the monomeric nitride carries two other possible acceptor orbitals, 2e and 3e. The nodal structure and extent in space of these is such that they might be thought to encourage attack by a nucleophile along the directions shown in **10** or **11**. A in **10** and C or D in **11** would correspond to the addition of

10 **11**

fifth ligand to the metal, not an unlikely reaction, since square-pyramidal L_4MN nitrides are known. Approach B, an attack at the nitride nitrogen, is an extremely interesting possibility. If the

(12) Elian, M.; Hoffmann, R. *Inorg. Chem.* **1975**, *14*, 1058.

(13) Chisholm, M. H.; Huffman, J. C.; Marchant, N. S. *J. Am. Chem. Soc.* **1983**, *105*, 6162.

attacking group were the N end of another nitride, one has the intriguing possibility of coupling two nitrides to a dinitrogen complex, **12**. Although **12** is unknown, Liebelt and Dehnicke

$$L_nM{\equiv}N + N{\equiv}ML_n \longrightarrow L_nM-N{\equiv}N-ML_n$$

12

have isolated an intermediate from reaction **13** which is believed to be $Cl_4Mo{\equiv}N-N{\equiv}MoCl_4$, on the basis of spectroscopic data.[14b]

$$2MoCl_5 + 2IN_3 \xrightarrow{\Delta} 2Cl_3MoN + 2Cl_2 + 2ICl + 2N_2$$

13

To form $Cl_3Mo{\equiv}N$, the N–N bond of the dimeric intermediate must break in a subsequent reaction representing the reverse of **12**. We will say more about this reaction later when we consider the L_4MN compounds.

The next logical step is the study of a hypothetical $(R_3W{\equiv}N)_2$ dimer of geometry **14** on the way to the known polymer structures. We will not report the detailed results here but only summarize the essential features. Extended Hückel calculations give an attractive potential energy curve for an approach of the two

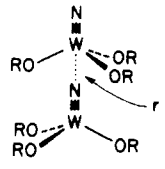

14

monomer units; in fact the optimum calculated r is too short, at 1.98 Å. The primary stabilizing interactions, between donor $2a_1$ of one monomer and acceptor $3a_1$ of the other, overcome assorted destabilizing interactions such as those between $2a_1$ orbitals of each unit, or the π orbitals of each.

To see clearly the symmetry restrictions that eventually make for M≡N bond alternation we must move to the polymer.

The $(RO)_3WN$ Linear Polymer

An important structural feature of the WL_3N (L = t-C_4H_9O) structure[11] **5** is the W–N···W bond alternation along the chain. The chain structure **5** can be regarded as distorted from an ideal WL_3N chain that has neither the W–N···W bond alternation nor the pyramidalization of WL_3 units. In general, an ideal ML_3X (X = N, O, etc.) chain **15** can be constructed from ML_3X_2 trigonal bipyramids by sharing the ligands X. The ML_3X chain **16a** results from **15** when M–X···M alternation is introduced. Pyramidalization of ML_3 units **16a** leads to **16b**. The latter captures the structural essence of **5**, except that the ML_3 units are arranged in the eclipsed manner. Our calculations show that conclusions regarding the eclipsed arrangement remain valid for the staggered WL_3 units in **5**. The eclipsed polymer is somewhat simpler to analyze.

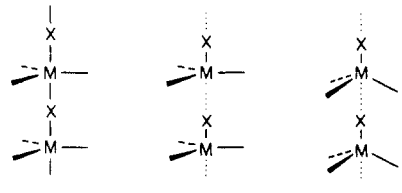

15 **16a** **16b**

The z^2 orbital of ML_3 interacts with the s, z orbitals of X to form σ bands. Formation of those bands can be easily explained

(14) Liebelt, W.; Dehnicke, K. *Z. Naturforsch*, **1979**, *B34*, 7.

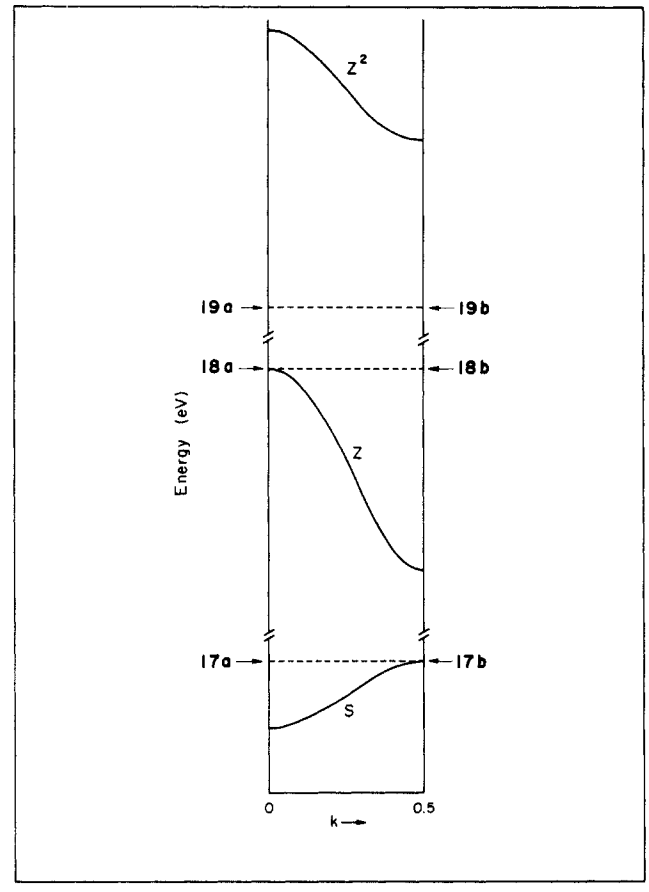

Figure 3. σ bands of ML_3X, **15** (schematic).

in terms of the s, z, and z^2 Bloch orbitals at the zone center (**17a**, **18a**, and **19a**, respectively) and those at the zone edge (**17b**, **18b**, and **19b**, respectively). At the zone center, **18a** does not interact either with **17a** or with **19a** by symmetry whereas the interaction between **17a** and **19a** does not vanish. At the zone edge, the interaction between **18b** and **19b** is allowed by symmetry while **17b** cannot interact either with **18b** or with **19b**. Since the overlap

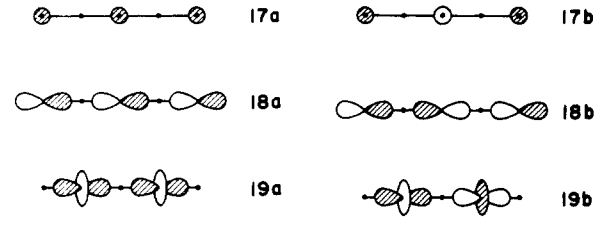

between z^2 and s is smaller than that between z^2 and z at a given M–X distance, we obtain the three σ bands shown schematically in Figure 3. Thus the z^2 orbital lowers the energy of the s band primarily in the region of the zone center but that of the z band in the region of the zone edge.

The xz orbital of ML_3 interacts with the x orbital of X leading to π bands and likewise for yz and y. Since the two sets of π bands are equivalent, we will only consider the π bands obtained from yz and y. The y and yz Bloch orbitals at the zone center are given by **20a** and **21a**, respectively. By symmetry, **20a** and **21a** do not interact while **20b** and **21b** do. Thus the resulting y and yz bands may be given schematically as shown in Figure 4. This reveals that the yz orbital lowers the energy of the y band in the region of the zone edge.

The above discussion shows that the high symmetry of **15** prohibits the d orbitals of ML_3 from stabilizing the s, p bands of the bridging ligands depending upon the value of the wavevector and the orbitals involved. Let us now examine how the σ, π bands of **15** are affected by the sequential structural distortion of bond alternation and pyramidalization **15** → **16a** → **16b**. We also return

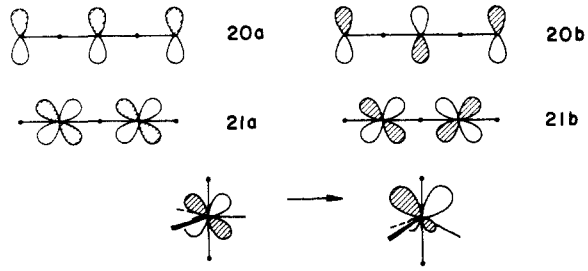

22

to the specific case of X = N, the nitride linear polymer.

When bond alternation is introduced, the interaction between **20a** and **21a** does not vanish anymore, so that the *yz* orbital can stabilize the *y* band in the vicinity of the zone center as well. As the ML_3 units are pyramidalized (i.e., **16a** → **16b**), the *yz* orbital of ML_3 (its *xz* orbital as well) is hybridized as schematically shown in **22**. Thus the π-interaction between the ML_3 and N units across the M–N bond is enhanced by the **16a** → **16b** distortion, thereby further lowering the energy of the *y* band. Parts a and b of Figure 5 show the π bands of $(HO)_3WN$ calculated for the structures **15** and **16b**, respectively. The *x*, *y* bands of nitrogen become significantly stabilized by the **15** → **16b** distortion, and at the same time the *xz*, *yz* bands of WL_3 are raised in energy. A phenomenon similar to the above may be considered to occur for the σ bands of Figure 4 during the **15** → **16b** distortion. Namely, it may be anticipated that, due to the low symmetry of **16b**, the z^2 orbital would lower the *z* band at the zone center and that of the s band at the zone edge. However, this picture is valid only when contribution of the ligands L to the valence orbitals of ML_3 is negligible. The calculated s, *z* bands of WL_3N (L = OH) for the structures **15** and **16b** are shown in Figure 6, a and b, respectively. The **15** → **16b** distortion is found to lower the s band but raise the *z* band. The latter is due largely to the involvement of the orbitals of L.

In Figure 6 the energy lowering of the s band is nearly cancelled by the energy raising of the *z* band, thus the overall energy of the σ bands does not vary significantly during the **15** → **16b** distortion. Consequently, the primary cause for the combined alternation and pyramidalization in the ML_3X chain is in the π-interactions. With respect to **15**, the stability of **16b** results from the orbital mixing of *yz* into *z* (and that of *xz* into *x*), which are of different energy. Thus the net distortion is an extended chain counterpart of a second-order Jahn–Teller distortion.[15]

Even though we cannot quantitatively reproduce W–N bond lengths (W≡N bond lengths calculated by varying only the tungsten–nitrogen distances are almost 0.8 Å too short (0.95 A)) we can discuss qualitatively the bond length alternation in various compounds. The second-order Jahn–Teller effect operates if a distortion to a lower symmetry structure causes a large HOMO–LUMO mixing. Second-order perturbation theory shows that orbital mixing is largest between orbitals with good overlap and a small energy difference.[15] For the nitrides, the orbital energy difference at the zone center can be tuned by changing either the bridging atom or the co-ligands. Substituting a less electronegative atom for the nitride bridge would increase the distortion by raising the HOMO energy. Changing from π-donor alkoxide ligands to σ-donors or π-acceptors would lower the LUMO energy and also increase the magnitude of distortion. We will return to this point when we treat the C_{4v} ML_4X structures.

The ML_4N Monomers

Consider now the building blocks of the trans corner-linked octahedral polymers, the square-pyramidal ML_4N molecules.

(15) For reviews of the Jahn–Teller effect in molecules and solids, see: (a) Englman, R. "The Jahn–Teller Effect in Molecules and Crystals"; Wiley-Interscience: New York, 1972. (b) Bersuker, I. B. "The Jahn–Teller Effect and Vibronic Interactions in Modern Chemistry"; Plenum Press: New York, 1984. (c) Burdett, J. K. *Appl. Spectrosc.Rev.* **1970**, *4*, 43.

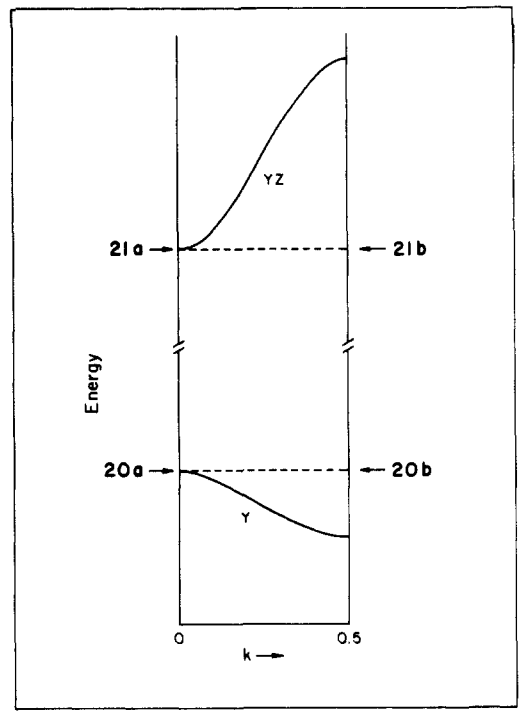

Figure 4. π bands of ML_3X, **15** (schematic).

X-ray crystal structures are available for a number of nitride monomers (M = Cr, Mo, W, Mn, Tc Re, Ru, Os)[16] and all but one show approximate C_{4v} symmetry with the nitrogen occupying the apex of the square pyramid. The lone exception[17] has been described as containing a $WNCl_2F_2^-$ trigonal bipyramid with the nitrogen in an equatorial position. The square-pyramidal nitrides all show the short metal–nitrogen bonds and pyramidalization about the metal characteristic of M–N multiple bonding. In a typical d^0 nitride such as $MoNCl_4^-$, the angle θ in **23** is 101.5–103°, a value close to those usually found for other d^0 square-pyramidal molecules.[18]

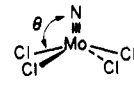

23

(16) (a) Cr^V d^1: Groves, J. T.; Takahashi, T.; Butler, W. M. *Inorg. Chem.* **1983**, *22*, 884. (b) Mo^{VI} d^0: (i) Fenske, D.; Liebelt, W.; Dehnicke, K. *Z. Anorg. Allg. Chem.* **1980**, *467*, 83. (ii) Müller, U.; Schweda, E.; Strähle, J. *Z. Naturforsch.* **1983**, *B38*, 1299. (iii) Knopp, B.; Lörcher, K.-P.; Strähle, J. *Z. Naturforsch.* **1977**, *B32*, 1361. (iv) Dehnicke, K.; Krueger, N.; Kujanek, R.; Weller, F. *Z. Kristallogr.* **1980**, *153*, 181. (v) Dehnicke, K.; Schmitte, J.; Fenske, D. *Z. Naturforsch.* **1980**, *B35*, 1070. (c) Mo^V d^1: (i) Schmitte, J.; Friebel, C.; Weller, F.; Dehnicke, K. *Z. Anorg. Allg. Chem.* **1982**, *495*, 148. (ii) Schweda, E.; Strähle, J. *Z. Naturforsch.* **1981**, *B36*, 662. (d) Mn^V d^2: (i) Hill, C. L.; Hollander, F. J. *J. Am. Chem. Soc.* **1982**, *104*, 7318. (ii) Buchler, J. W.; Dreher, C.; Lay, K.-L.; Lee, Y. J.; Scheidt, W. R. *Inorg. Chem.* **1983**, *22*, 888. (e) Tc^V d^2: Baldas, J.; Bonnyman, J.; Pojer, P. M.; Williams, G. A.; Mackay, M. F. *J. Chem. Soc., Dalton Trans.* **1981**, 1798. (f) Re^{VI} d^1: (i) Kafitz, W.; Weller, F.; Dehnicke, K. *Z. Anorg. Allg. Chem.* **1982**, *490*, 175. (ii) Liese, W.; Dehnicke, K.; Rogers, R. D.; Shakir, R.; Atwood, J. L. *J. Chem. Soc., Dalton Trans.* **1981**, *1061*. (g) Re^V d^2: (i) Doedens, R. J.; Ibers, J. A. *Inorg. Chem.* **1967**, *6*, 204. (ii) Fletcher, S. R.; Skapski, A. C. *J. Chem. Soc., Dalton Trans.* **1972**, 1079. (iii) Fletcher, S. R.; Rowbottom, J. F.; Skapski, A. C.; Wilkinson, G. *J. Chem. Soc., Chem. Commun.* **1970**, 1572. (h) Ru^{VI} d^2: (i) Phillips, F. C.; Skapski, A. C. *Acta Crystallogr.* **1975**, *B31*, 2667. (ii) Collison, D.; Garner, C. D.; Mabbs, F. E. *J. Chem. Soc., Dalton Trans.* **1981**, 1820. (i) Os^{VI} d^2: (i) Phillips, F. L.; Skapski, A. C. *J. Cryst. Mol. Struct.* **1975**, *5*, 83. (ii) Collison, D.; Garner, C. D.; Mabbs, F. E.; Salthouse, J. A.; King, T. J. *J. Chem. Soc., Dalton Trans.* **1981**, 1812. (iii) Phillips, F. L.; Skapski, A. C.; Withers, M. J. *Transition Met. Chem. (Weinheim, Ger.)* **1975–1976**, *1*, 28.

(17) W^{VI} d^0 (trigonal bipyramidal): Fenske, D.; Kujanek, R.; Dehnicke, K. *Z. Anorg. Allg. Chem.* **1983**, *507*, 51.

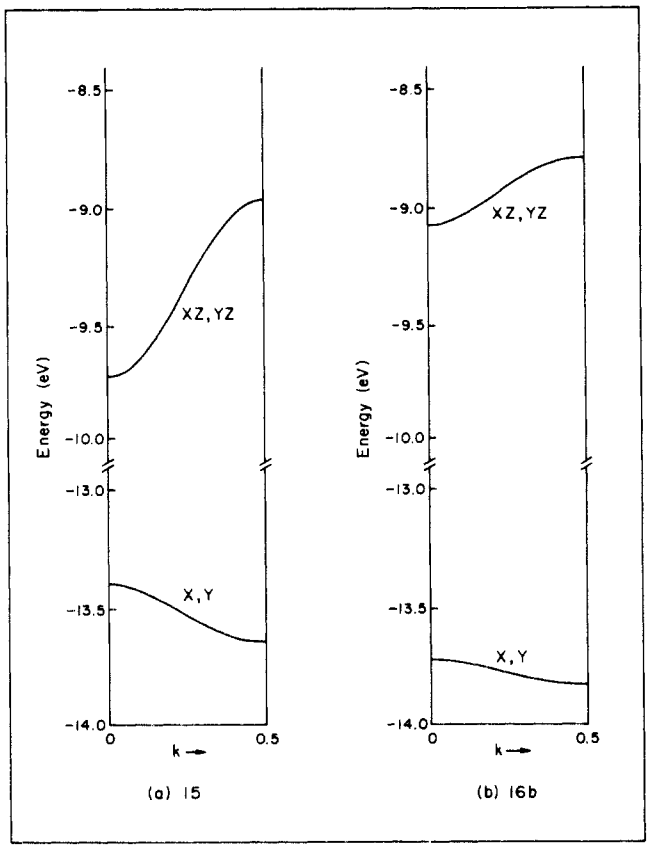

Figure 5. π bands of $(HO)_3WN$.

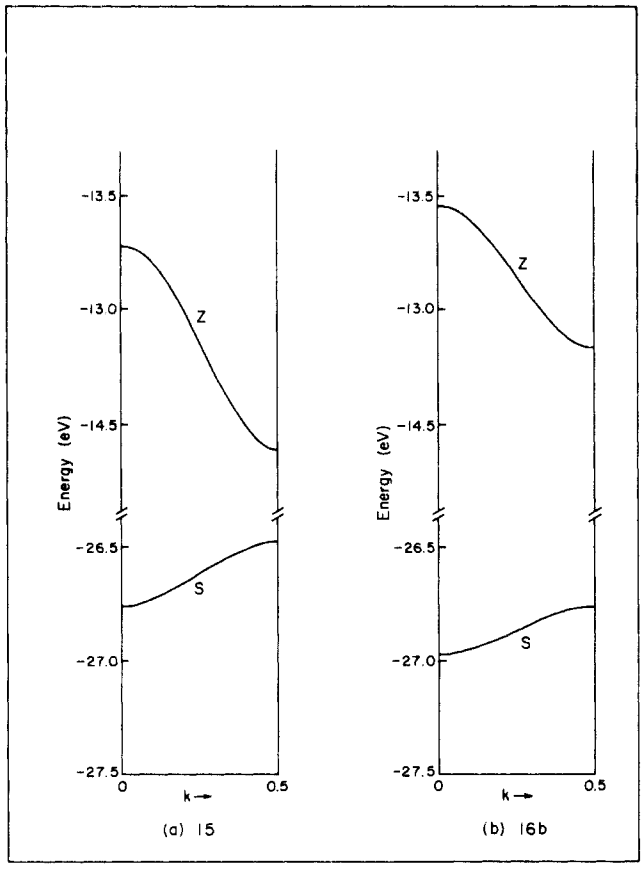

Figure 6. σ bands of $(HO)_3WN$.

Although the bonding within C_{4v} ML_5 molecules has been presented before[19,20] we need to discuss it again to establish the

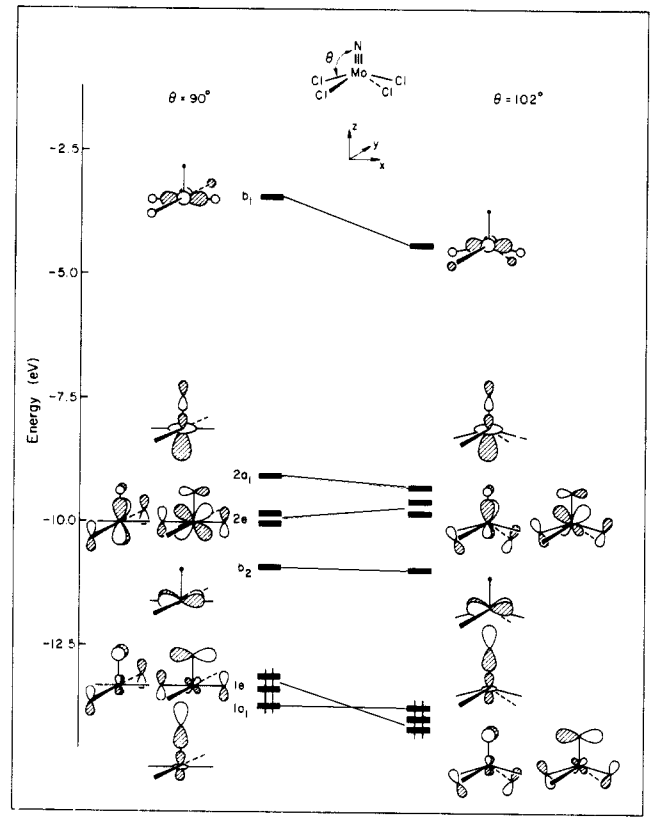

Figure 7. Correlation diagram showing the effect of pyramidalization on the orbitals of $MoNCl_4^-$. Geometry on the right, $\theta = 102°$, is the calculated energy minimum obtained by varying θ.

level ordering within the nitride d block. These levels are shown on the left in Figure 7 for $MoNCl_4^-$ with $\theta = 90°$.

The splitting pattern of four d orbitals below one is characteristic of square-planar or square-pyramidal complexes. The higher a_1 is a hybrid of z^2 and z, **24** directed toward the open coordination site. The xy orbital is raised in energy by π bonding with the basal chloride ligands. The stronger π-donor ability of the nitride has

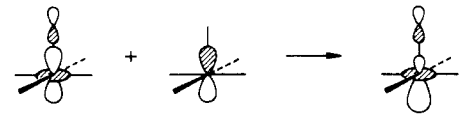

24

pushed xz and yz higher still. If we assign the nitride a 3- oxidation state, the molybdenum is Mo^{VI}, d^0, and all the d orbitals are empty. The HOMO's are a degenerate pair of metal–ligand π-bonding orbitals, mainly on the ligands, with a nitrogen-localized lone pair immediately below.

The right side of Figure 7 shows the effect of pyramidalizing $MoNCl_4^-$ to the minimum energy C_{4v} geometry with $\theta = 102°$. The figure shows only the empty d block and first few occupied orbitals, but energy changes within the antibonding d orbitals reflect energy changes within the lower, bonding orbitals. Bending the chloride ligands down in the nodal planes of the xy orbital leaves this lowest d orbital relatively unchanged in energy. xz and yz rise in energy because of two effects: Mo–Cl σ^* and increased Mo–N π^* interactions. This occurs as basal ligand orbitals are allowed to mix with xz and yz in a σ-antibonding way. The metal xz and yz hybridize away from the chlorides and toward the apical nitride ligand as in **25**. The hybridization reduces the unfavorable Mo–Cl σ^* interaction at the expense of increased

(18) Holmes, R. R. *Prog. Inorg. Chem.* **1984**, *32*, 216.

(19) (a) Rossi, A. R.; Hoffmann, R. *Inorg. Chem.* **1975**, *14*, 365. (b) Albright, T. A. *Tetrahedron* **1982**, *38*, 1339. (c) Albright, T. A.; Burdett, J. K.; Whangbo, M.-H. "Orbital Interactions in Chemistry"; John Wiley: New York, 1984; Chapter 17.

(20) DuBois, D. L.; Hoffmann, R. *Nouv. J. Chim.* **1977**, *1*, 479.

25

Mo–N π^* character. Bending down the Cl ligands also reduces out-of-plane Mo–Cl π bonding by decreasing π overlap. Decreased σ^* interaction is responsible for the energy lowering of z^2 and $x^2 - y^2$. Corresponding changes are observed in the σ- and π-*bonding* orbitals. The increased Mo–N π bonding is evident in Figure 7; the degenerate pair of metal–ligand π-bonding orbitals drops below the nitrogen lone pair. This nitrogen lone pair becomes the HOMO of the pyramidal $MoNCl_4^-$.

The orbital energy level diagram of Figure 7 has received some theoretical and experimental support. Extended Hückel calculations for $RuNCl_4^-$ with $\theta = 90°$ show the same level ordering but different orbital compositions and energy level splittings.[20] ESR and ^{14}N ENDOR experiments on the d^1 compounds CrN(OEP) and CrN(TTP) show that the unpaired electron occupies the metal xy orbital,[21] the calculated LUMO for d^0 $MoNCl_4^-$. Our interpretation of Figure 7 agrees with the bonding description inferred from EPR measurements on $ReNCl_4^-$. These experiments indicate strong metal–nitrogen π bonding but weak out-of-plane π bonding between Re and Cl.[22] This is consistent with the metal being above the basal plane of the four chloride ligands.

The low-lying a_1 acceptor orbital dominates the chemistry of these compounds, whereas the HOMO confers upon the nitrogen only a weak electron-donating ability.[5a] Nor does the nitride ligand act as a strong nucleophile. We know of only one clear-cut case of nucleophilic attack by the nitrogen atom of a five-coordinate transition-metal nitride.[23] In fact, the small nitrogen component in the acceptor orbital $2a_1$ often determines reactivity at the nitrogen. Compounds with the formula $L_4M{\equiv}N$ (M = Re, Ru, Os) react with 2 equiv of phosphine to give $L_4(PR_3)M{\equiv}NPR_3$.[24] Phosphineiminato complexes of the early transition metals Ti, V, Nb, Ta, Mo have also been made, though not from the corresponding nitrides.[25] In contrast to their rather limited reactivity at the nitrogen atom, the nitrides readily add a sixth ligand to restore octahedral coordination about the metal. X-ray crystal structures show unusually long metal–ligand bonds trans to the nitrogen,[26] so that the six-coordinate nitrides retain some character of the L_4MN complexes.

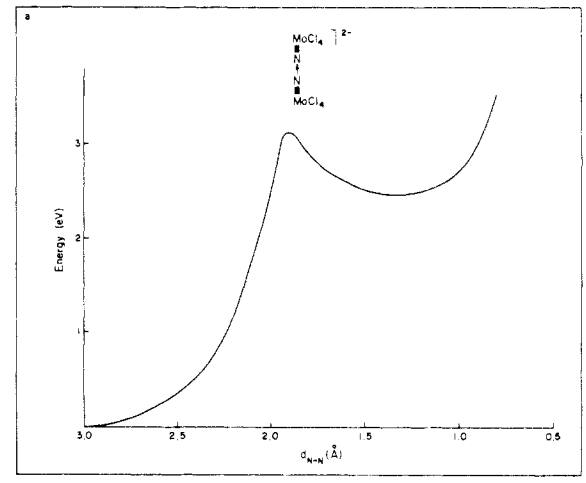

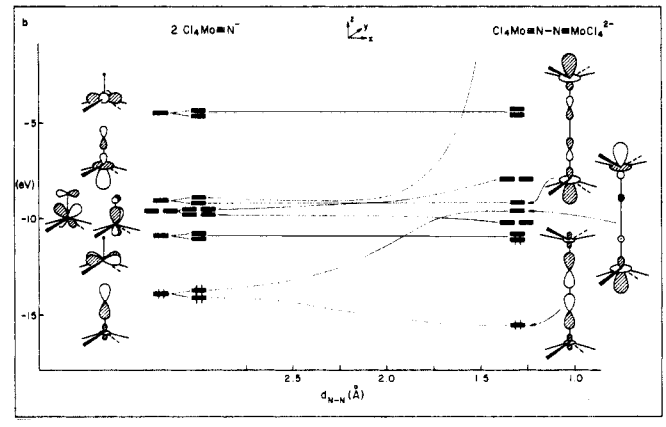

Figure 8. (a) Potential energy curve for the approach of two $Cl_4Mo{\equiv}N^-$ molecules to give a μ-dinitrogen complex. The energy zero represents the energy of two separated Cl_4MoN molecules. (b) Correlation diagram showing the avoided crossing of a_1 orbitals that gives rise to the energy barrier in (a). The energy ordering $2a_1$ below $3a_1$ can be understood in terms of through-bond coupling between N_2 σ^* and the antisymmetric combination of metal z^2 (and N_2 σ with the symmetric combination).

We studied in detail distortions of the square-pyramidal geometry by performing a series of Berry pseudorotations[27] to interconvert square-pyramidal and trigonal-bipyramidal geometries, with the nitrogen at the apex or the base of the square pyramid and axial or equatorial positions of the trigonal bipyramid. We calculate that the experimentally observed square-pyramidal geometry is only 3 kcal/mol more stable than the trigonal bipyramid with equatorial nitrogen. Apparently effects other than the simple electronic factors considered here provide this extra 3-kcal/mol stabilization for the one molecule[17] known to adopt this trigonal-bipyramidal structure. There also appears to be a local minimum, albeit at higher energy, for a trigonal bipyramid with nitrogen axial.

A Walsh diagram for the metal d block under pseudorotation was also constructed, but it is not shown here. It allows us to reach some conclusions concerning the ease of this deformation for d electron counts greater than 0. Level crossings for d^{3-7} indicate that interconversion of the two square-pyramidal structures is symmetry forbidden for these electron counts. Pseudorotation should be expecially facile for d^{0-2}, whereas a large barrier to the square-pyramidal interconversion appears at $d^{9,10}$.

Just as in the case of L_3MN we should note the alternative acceptor capabilities of the L_4MN unit, namely utilizing the e or b_2 orbitals of Figure 7. In fact, calculations show minima corresponding to bound dimers only for the approach of two $Cl_4Mo{\equiv}N^-$ units as shown in **26** and **27**. Surfaces for other geometries—**28** through **31**—are always repulsive because of interactions with chlorine lone pair orbitals. The Mo–N distance

(21) Buchler, J. W.; Dreher, C.; Lay, K.-L.; Raap, A.; Gersonde, K. *Inorg. Chem.* **1983**, *22*, 879.
(22) Lack. G. M.; Gibson, J. F. *J. Mol. Struct.* **1978**, *46*, 299.
(23) Groves, J. T.; Takahashi, T. *J. Am. Chem. Soc.* **1983**, *105*, 2073.
(24) (a) Wright, M. J.; Griffith, W. P. *Transition Met. Chem.* (*Weinheim, Ger.*) **1982**, *1*, 53. (b) Pawson, D.; Griffith, W. P. *J. Chem. Soc., Dalton Trans.* **1975**, 417. (c) Pawson, D.; Griffith, W. P. *Inorg.* Nucl. *Chem. Lett.* **1974**, *10*, 253. (d) Griffith, W. P.; Pawson, D. *J. Chem. Soc., Chem. Commun.* **1973**, 418. (e) Dehnicke, K.; Prinz, H.; Kafitz, W.; Kujanek, R. *Liebigs Ann. Chem.* **1981**, 20. (f) Phillips, F. L.; Skapski, A. C. *J. Chem. Soc., Dalton Trans.* **1978**, 1448. (g) Mronga, N.; Weller, F.; Dehnicke, K. *Z. Anorg. Allg. Chem.* **1983**, *502*, 35.
(25) (a) Choukroun, R.; Gervais, D.; Dilworth, J. R. *Transition Met. Chem.* (*Weinheim, Ger.*) **1978/81**, *4*, 249. (b) Dilworth, J. R.; de Liefde Meijer, H. J.; Teuben, J. H. *J. Organomet. Chem.* **1978**, *159*, 47. (c) Müller, U.; Dübgen, R.; Dehnicke, K. *Z. Anorg. Allg. Chem.* **1981**, *473*, 115. (d) Dübgen, R.; Müller, U.; Weller, F.; Dehnicke, K. *Z. Anorg. Allg. Chem.* **1980**, *471*, 89. (e) Bezler, H.; Strähle, J. *Z. Naturforsch.* **1979**, *B34*, 1199. (f) Scott, D.; Wedd, A. G. *J. Chem. Soc., Chem. Commun.* **1974**, 527.
(26) (a) Mo^{VI} d^0: Schweda, E.; Strähle, J. *Z. Naturforsch.* **1980**, *B35*, 1146. (b) Mo^{IV} d^2: Dilworth, J. R.; Dahlstrom, P. L.; Hyde, J. R.; Zubieta, J. *Inorg. Chim. Acta* **1983**, *71*, 21. (c) Tc^{V} d^2: Baldas, J.; Bonnyman, J.; Williams, G. A. *J. Chem. Soc., Dalton Trans.* **1984**, 833. (d) Re^{VII} d^0: Kafitz, W.; Dehnicke, K.; Schweda, E.; Strähle, J. *Z. Naturforsch.* **1984**, *B39*, 1114. (e) Re^{VI} d^1: de C. T. Carrondo, M. A. A. F.; Shakir, R.; Skapski, A. C. *J. Chem. Soc., Dalton Trans.* **1978**, 844. (f) Re^{V} d^2: Corfield, P. W. R.; Doedens, R. J.; Ibers, J. A. *Inorg. Chem.* **1967**, *6*, 197. (g) Os^{VI} d^2: (i) Bright, D.; Ibers, J. A. *Inorg. Chem.* **1969**, *8*, 709. (ii) Atovmyan, L. O.; Tkachev, V. V. *Zh. Strukt. Khim.* **1968**, *9*, 708; *J. Struc. Chem.* **1968**, *9*, 618. (iii) Atovmyan, L. O.; Tkachev, V. V. *Zh. Strukt. Khim.* **1970**, *11*, 933. *J. Struct. Chem.* (*Engl. Transl.*) **1970**, *1*, 868. (iv) Atovmyan, L. O.; Bokii, G. B. *Zh. Strukt. Khim.* **1960**, *1*, 501; *J. Struct. Chem.* (*Engl. Transl.*) **1960**, *1*, 468. (v) Tkachev, V. V.; Krasochka, O. N.; Atovmyan, L. O. *Zh. Strukt. Khim.* **1976**, *17*, 940; *J. Struct. Chem.* (*Engl. Transl.*) **1976**, *17*, 807.

(27) (a) Berry, R. S. *J. Chem. Phys.* **1960**, *32*, 933. (b) Berry, R. S. *Rev. Mod. Phys.* **1960**, *32*, 447.

26 **27**

calculated for **26** (2.40 Å) is quite close to the long Mo–N distance in the square tetramers (2.15–2.20 Å).[6]

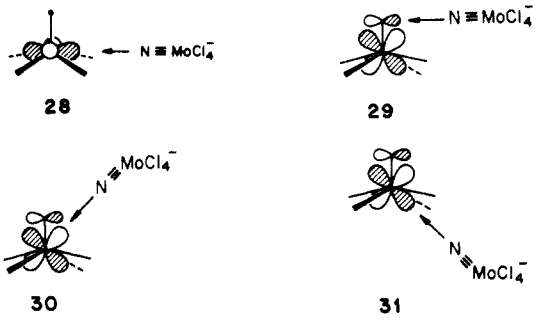

28 **29**

30 **31**

The energy as a function of nitrogen separation for the nitrogen coupling reaction **27** is shown in Figure 8. The calculated equilibrium N–N distance is 1.35 Å in the bound minimum. A recent theoretical study of the dimerization of *neutral* Cl_4MoN by Rappé[28] indicated the existence of two N–N bonded minima, a more stable one with Mo–N = 2.26 Å and N–N = 1.11 Å, and another one with Mo–N = 1.80 Å and N–N = 1.23 Å. The system studied by Rappé does not dissociate to isolated nitrido structures because in doing so it would have to go to "Mo(VII)," or remove electrons from the N lone pairs. If we remove two electrons from the system of Figure 8 and keep Mo–N at 1.66 Å, we obtain the same optimum N–N separation for neutral $(Cl_4MoN)_2$, 1.35 Å, as we calculated for $(Cl_4MoN)_2^{2-}$. This is because the two electrons are removed from the nonbonding HOMO of $(Cl_4MoN)_2^{2-}$. As Rappé also noted, $(Cl_4MoN)_2$ is an isolable intermediate in the $MoNCl_3$ synthesis, **13**.[14] This minimum suggests the fascinating possibility of coupling two $L_4M{\equiv}N^-$ units to make a μ-dinitrogen complex. The large energy barrier that must be overcome for this approach is due to the intended correlation of the antisymmetric combination of nitrogen z orbitals with the N–N σ^* orbital in the product (see Figure 8b). The avoided crossing in Figure 8b is removed and the reaction barrier lowered slightly by tipping the incoming $Cl_4Mo{\equiv}N^-$ unit to a position intermediate between **27** and **29**. The energy is lowered in the early stages of the coupling reaction because it is energetically more favorable to orient the reactants for good overlap between donor $2a_1$ and acceptor e orbitals while minimizing repulsion between filled orbitals. Such a synthetic strategy—coupling two $L_4M{\equiv}N$ molecules to make a dinitrogen complex—should be most favorable if M is a late transition metal so that the nitrogen component of the acceptor orbitals is as large as possible.

Obviously, our calculated energies and bond lengths are not quantitatively correct, but comparing the energies of approach for the geometries shown in **26**–**31** shows the preeminence of the $2a_1$ acceptor orbital in stabilizing the oligomeric or polymeric reaction products. Of course the tetramer formation we will eventually examine could be viewed as the outcome of a chain of donor–acceptor interactions, using one or another R_4MN conformation. But let us discuss the linear polymer first.

MXL_4 Polymers

We will look at MXL_4 polymers from a more general vantage point than that offered by the nitride systems alone. Nevertheless, the nitride system, $^1_\infty[MoNCl_4^-]$, is a convenient example for extracting the features we are pursuing. The energy bands for the *idealized* $MoNCl_4^-$ polymer with all equal Mo–N bond lengths and with N–Mo–Cl angles set equal to 90° are shown in Figure 9a. The high energy z^2 and x^2-y^2 orbitals are relatively unimportant and are omitted from the Figure. In Figure 9b the computed energy bands for a distorted $MoNCl_4^-$ chain are displayed. The N-Mo-Cl angle θ was fixed at 102°, and alternating long (2.17Å) and short (1.67 Å) Mo–N bond lengths were used.

The principal features of the $^1_\infty[MoNCl_4^-]$ system can be understood in exactly the same terms as were employed for the $(RO)_3WN$ chain discussed earlier. For the symmetrical chain (Figure 9a) the center of the Brillouin zone possesses nitrogen σ and π lone pairs of a_{1u} and e_g symmetry as the highest filled bands. Relative to the $MoNCl_4^-$ monomer, the σ lone pair has been stabilized by a bonding interaction with metal orbitals. Since the chain has D_{4h} point symmetry at both Mo and N sites, the N p_z orbital mixes only with Mo z at $k = 0$ and with z^2 or s at $k = 0.5(\pi/a)$, as depicted in **33**. This state of affairs is obviously analogous to our previous discussion of the ML_3X chain and the

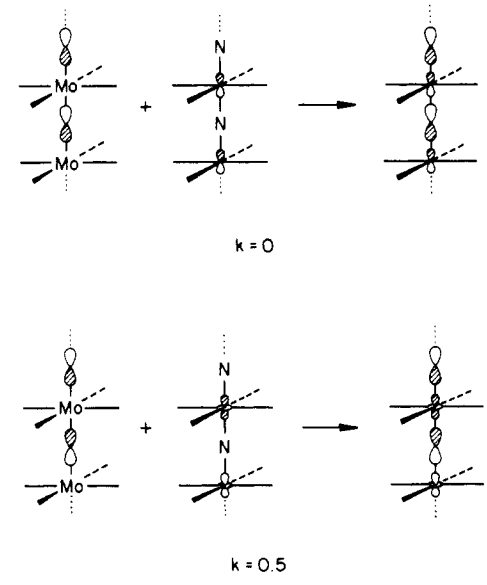

32

orbitals given in **17**–**19**. The π bands also parallel those found for the $^1_\infty[ML_3X]$ system and the reader may refer to our discussion of that chain and illustrations **20**–**22** for the important e bands of Figure 9. Only the xy and $x^2 - y^2$ bands are significantly altered in moving from the trigonal-bipyramidal chain to the octahedral chain, but these bands do not contribute to Mo–N bonding in any case because of their δ symmetry with respect to the chain axis. Thus, the xy orbital gives rise to a flat nonbonding b_2 band which does not significantly change upon distortion of the chain. It is the partial occupation of this band which gives rise to the interesting magnetic properties in the d^1 compound α-$VOSO_4$.[8b]

The driving force for distorting the ML_4X chain to yield an asymmetrically bridged polymer is the same as that for the ML_3X case, namely the mixing of metal $d_{xz,yz}$ bands with bridging ligand $p_{x,y}$ bands (at $k = 0$). This leads to a stabilization of the occupied nitrogen x, y bands. We have performed calculations on a number of model systems to examine the influence ligands and bridging atoms have on the distortion. The results are summarized in Table I. For all the model systems, energy differences were calculated for the distortion where the long to short M–X distance ratio was 11:9. The M–M distance was kept constant in moving from the equidistant case to the distorted case. The extent of distortion is typical for that found in various oxide systems (e.g., $WOCl_4$,[29a]

(28) Rappé, A. K. *Inorg. Chem.* **1984**, *23*, 995.

(29) (a) Hess, H.; Hartung, H. *Z. Anorg. Allg. Chem.* **1966**, *344*, 157. (b) Müller, U. *Acta Crystallogr.* **1984**, *C40*, 915.

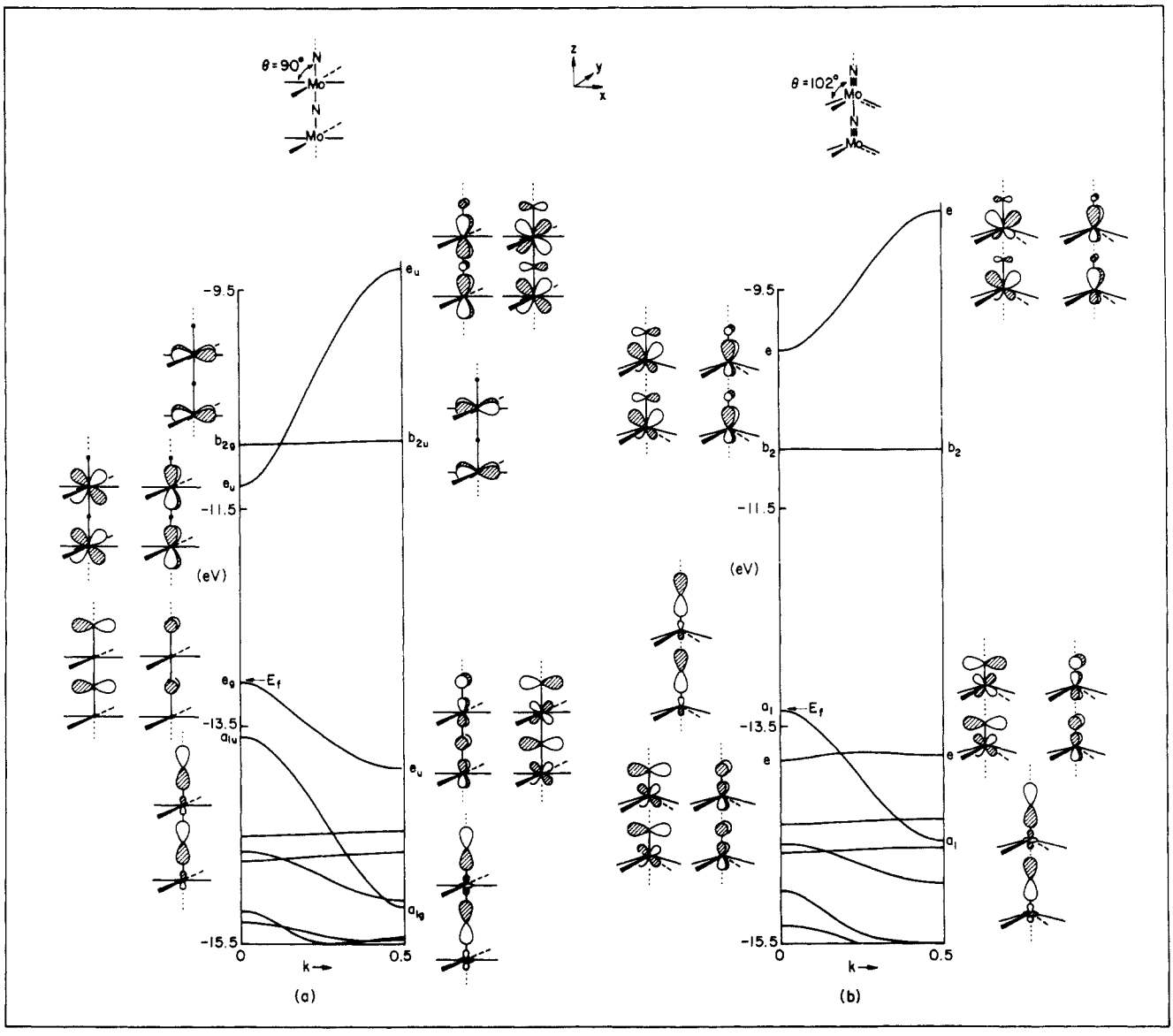

Figure 9. Band structures of polymeric $MoNCl_4^-$ showing HOMO–LUMO mixing at $k = 0$ when the point symmetry is lowered from D_{4h} (a) to C_{4v} (b) by introducing Mo–N bond length alternation and pyramidalizing about the metal.

Table I. Results for Distortion of Model ML_4X Chains[a]

$^1_\infty[NbH_4X]$ X	d° results l, Å	Nb–H = 1.7 Å ΔE_{tot}, eV	ΔE_π, eV	ΔE_σ, eV
N	1.92	−0.651	−0.775	+0.124
O	1.92	−0.472	−0.554	+0.082
F	2.07	−0.346	−0.373	+0.027
S	2.25	−0.931	−1.101	+0.170
$^1_\infty[NbCl_4X]$ X	d° results l, Å	Nb–Cl = 2.35 Å ΔE_{tot}, eV	ΔE_π, eV	ΔE_σ, eV
N	1.92	−0.356	−0.479	+0.123
O	1.92	−0.203	−0.264	+0.061
F	2.07	−0.104	−0.096	−0.008
S	2.25	−0.553	−0.712	+0.159

[a] In all cases the distance l is the length of the M–X bonds in the undistorted chains and distorted chains had long and short alternating distances of $1.1l$ and $0.9l$.

$WOBr_4$,[29b] and tetragonal $BaTiO_4$). Pyramidalization of the ML_4 square-planar unit was included with $\theta = 94.42°$ for L = Cl and $\theta = 94.62°$ for L = H. The metal was taken to be Nb for all calculations, and the electron count was chosen to give a d^0 configuration for the metal.

The trends in Table I reveal some strengths and weaknesses of our treatment of this problem. First, in either MH_4X or MCl_4X chains, the tendency to distort increases with the decreasing electronegativity of the nonmetal bridging atom (S > N > O > F). This is consistent with the experimental findings; in $WOBr_4$ and $WOCl_4$ the W–X distance differentials are respectively 0.38 and 0.40 Å while in $ReNCl_4$ it is 0.90 Å. When the energy change is decomposed into its σ and π parts (ΔE_π and ΔE_σ), we obtain the expected result that the π bands are indeed responsible for driving the distortion. Less electronegative bridging atoms result in a similar p–d "HOMO–LUMO" gap and the second-order Jahn–Teller distortion is accentuated. Comparison of the Cl-substituted polymer with the model H-substituted chain shows the influence of the Cl ions' modest role as a π donor: the $d_{xz,yz}$ bands are pushed up and delocalized onto the Cl ligands and hence interact more poorly with the $p_{x,y}$ orbitals of the bridging atom. It can be seen that the major differences are in the π component of the energy, ΔE_π. The tendency for bond alternation does not significantly depend on the ligands' σ-donating capacity. We feel that the major deficiency of our treatment is quantitative: the σ electrons provide a restoring force resisting the M–X bond alternation that is too small. For example, even for the fluoride bridged chains we calculate a small stabilization upon distortion, yet perovskite ScF_3 and the tetramer $(MoF_5)_4$ contain only symmetrically bridging fluorides.

There are, to our knowledge, no instances of nitride or oxide bridged one-dimensional $^1_\infty[ML_nX]$ chains which exhibit *symmetric* bridging. Our treatment suggests that for electron counts greater than d^2, the symmetric alternative should be

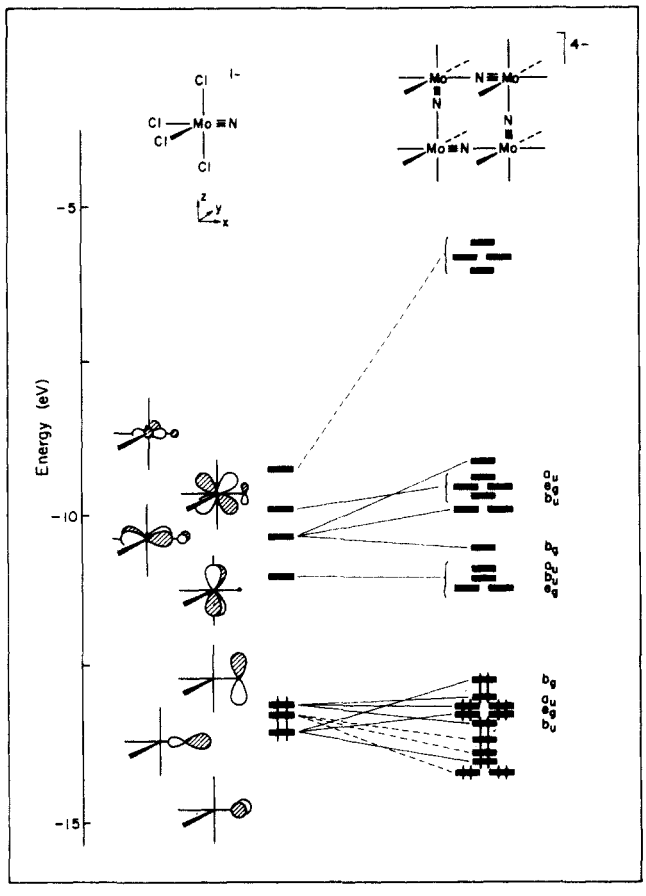

Figure 10. Interaction of four $MoNCl_4^-$ fragments to give $[MoNCl_4]_4^{4-}$.

stabilized—increasingly so with decreasing d electron concentration up to d^6. As the e ($d_{xz,yz}$) bands shown in Figure 13 become occupied the stabilization conferred by bond alternation is cancelled (the flat d_{xy} band takes the first two d electrons). Calculations on $^1_\infty[NbNCl_4]$ gave a crossover from the asymmetric to symmetric behavior for d^n with $n \cong 3$. If the σ restoring force is indeed *underestimated*, perhaps a symmetric chain can be prepared by only modest doping of a d^2 system with donors.

The $MoNCl_4^-$ Tetramer

Having analyzed the bonding in polymers of vertex sharing polyhedra arranged trans to one another, we turn to a discussion of cis corner-linked octahedral compounds. These Mo and W tetramers, described in the introduction, are faithfully represented by a model compound of C_{4h} symmetry, $[MoNCl_4^-]_4$, **33**. This hypothetical molecule can be "synthesized" by two different routes.

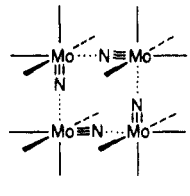

33

First, one could imagine bringing together four monomeric $MoNCl_4^-$ units to give the tetramer. Alternatively, one could construct the tetramer by interacting a fragment consisting of four $MoCl_4^{2+}$ units with a second fragment made up of the four N^{3-} ligands. The first approach, the more chemical one, shows what holds the tetramers together. The second view is useful for understanding the role played by the π orbitals in determining metal–nitrogen bond lengths.

Forming the $[MoNCl_4^-]_4$ tetramer from four $MoNCl_4^-$ units gives the orbital energy levels shown in Figure 10. As we anticipated in discussing the monomers, the four nitrogen lone-pair

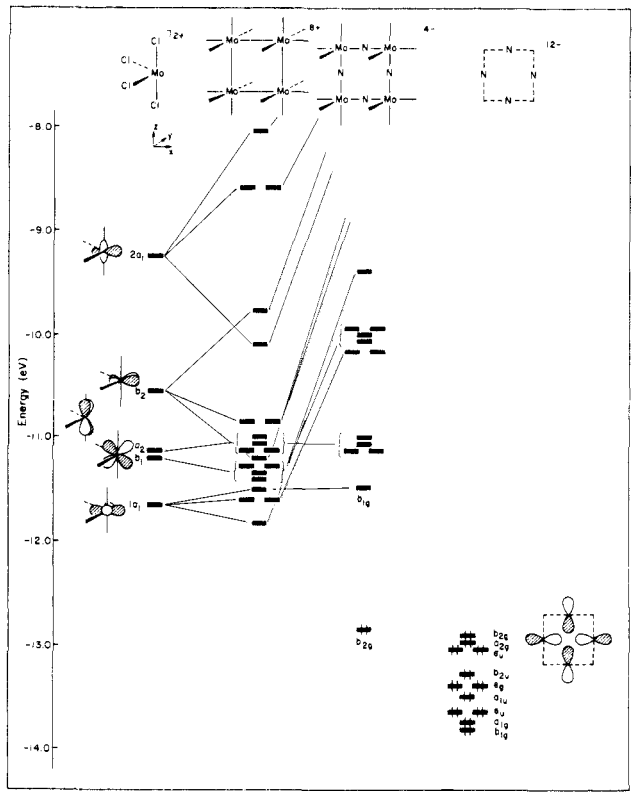

Figure 11. Interaction of four $MoCl_4^{2+}$ fragments to give $[MoCl_4]_4^{8+}$, followed by interaction with $[N]_4^{12-}$ to form $[MoNCl_4]_4^{4-}$. Product HOMO and LUMO orbitals are of different symmetries in D_{4h} and cannot mix.

orbitals interact with the Mo-based σ acceptors to give four σ-bonding levels and their antibonding counterparts. It is this σ interaction that drives tetramer formation, since the π interaction is a repulsive one. The repulsion is clearly seen in the π orbitals located in the molecular plane: only one orbital is bonding, but three are antibonding. In contrast, the out-of-plane π orbitals interact very little and contribute virtually nothing to the bonding between tetramers. The nature of these π orbitals, particularly those near the HOMO–LUMO gap, will be discussed later. For now we note only that the π interaction hinders tetramer formation.

To understand the role of the π orbitals in determining metal–nitrogen bond lengths we now construct the tetramer from a $[MoCl_4^{2+}]_4$ unit and a $[N^{3-}]_4$ fragment. Figure 11 shows how the orbitals of $[MoCl_4^{2+}]_4$ can be built up from those of the $MoCl_4^{2+}$ unit. On the left of the figure are the usual orbitals of the C_{2v} ML_4 unit[12,19b,c] oriented in an unconventional way. In our coordinate system the highest energy orbital ($2a_1$) is a combination of metal z^2 with some zy, whereas the b_2 orbital immediately below consists mainly of metal $x^2 - y^2$. In addition to their metal d character, these two metal–ligand σ^* orbitals contain some metal x and y. This serves to hybridize them away from the ligands and toward the two empty octahedral coordination sites along the x and y axes. The a_2 and b_1 orbitals are mixtures of metal xz and yz interacting with ligand orbitals in π^* fashion. The other π^* orbital, $1a_1$, consists of primarily molybdenum xy. $1a_1$ is therefore oriented for π bonding with ligands at both empty coordination sites.

We do not wish to draw out the 20 orbitals that form when four such $MoCl_4^{2+}$ units interact, as indicated in the left side of Figure 15. They split in straightforward, topologically determined ways, as a result of the weak, long-distance Mo–Mo interaction. The right side of Figure 15 shows the p levels of four N^{3-} atoms, also split just a little. The $(N^{3-})_4$ fragment presents a total of 16 orbitals—four s combinations are not shown in Figure 11. Fifteen of these 16 $(N^{3-})_4$ orbitals have the correct symmetry to interact effectively with 15 of the 20 $(MoCl_2^{4+})_4$ d block orbitals. Five metal levels and one nitrogen level do not interact, and these

combinations we do sketch in **34**. Since the nitrogen fragment

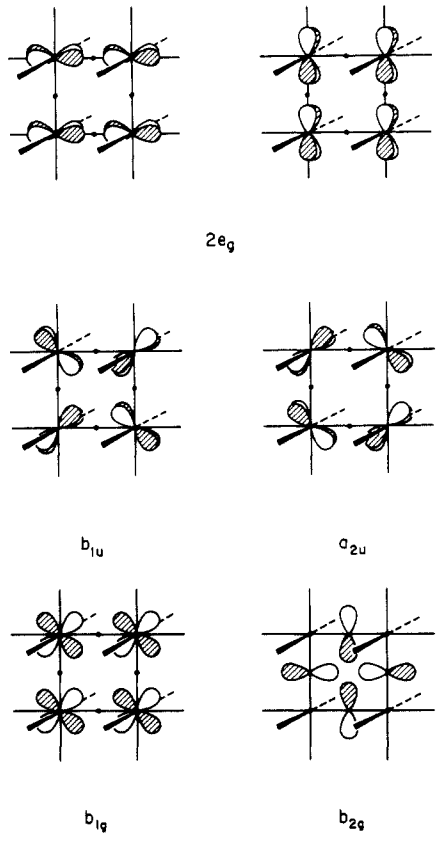

34

has no orbitals of a_{2u} or b_{1u} symmetry, these metal orbitals remain unchanged in energy. The same situation occurs for the nitrogen b_{2g}. Metal $2e_g$ simply has too many nodes to mix with nitrogen e_g. Nodal planes of $2e_g$ pass through the nitrogen atoms so the overlap of nitrogen e_g with $2e_g$ is zero. Since molybdenum b_{1g} is π and nitrogen b_{1g} is σ, these two orbitals also have zero overlap. As a result, neither these five metal orbitals nor the nitrogen b_{2g} can participate in π bonding. They form instead the highest occupied and lowest unoccupied molecular levels of the composite symmetrical tetranuclear nitride.

A normal mode analysis shows that a vibration of A_{2g} symmetry—required to mix metal b_{1g} with nitrogen b_{2g}—includes the nitrogen atom motion shown in **35**. The driving force for such a distortion is the HOMO–LUMO mixing evident in the Walsh diagram for bond alternation (Figure 12). Whereas these orbitals were of different symmetries in D_{4h}, in the new structure of C_{4h} symmetry both become b_g and their mixing is allowed. This

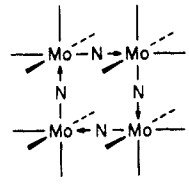

35

mixing of nearly degenerate HOMO and LUMO by a vibration of the proper symmetry is another (molecular) example of the second-order Jahn–Teller distortion to a lower symmetry structure. In this example, the result is increased π bonding and a thermodynamically more stable structure. We understand that a_{2u}, b_{1u}, and $2e_g$ remain at the same energy after distortion because they become the nonbonding members of the sets of three a_u, b_u, and e_g orbitals. They each become trapped between bonding and antibonding levels of the same symmetry.

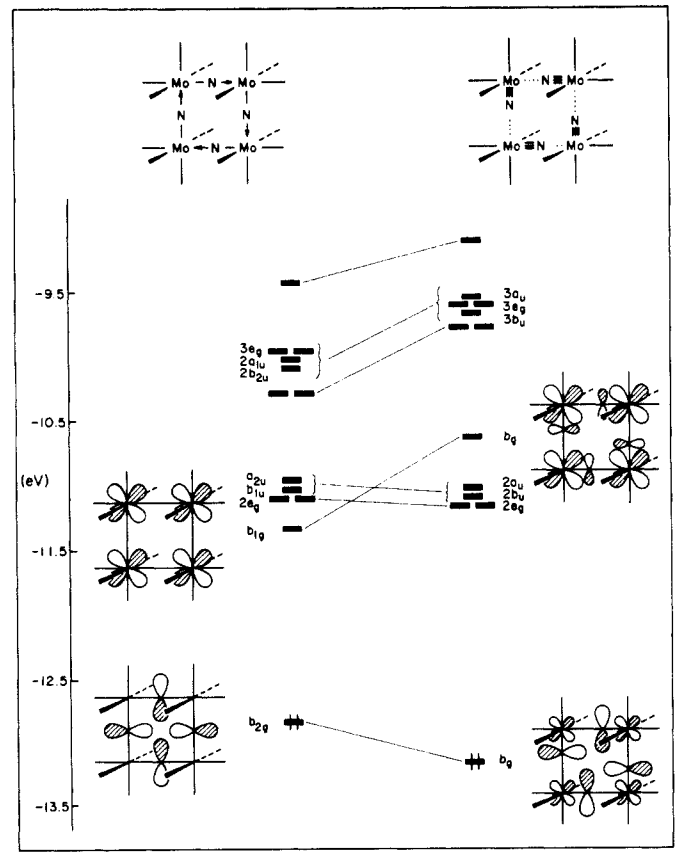

Figure 12. Correlation diagrams showing the mixing of Mo-based b_{1g} and N-localized b_{2g} upon lowering symmetry from D_{4h} to C_{4h} as shown above.

The transformation pictured in **35** involves shifting each nitrogen atom toward alternate corners of the square. In our model compound, moving the nitrogen atoms toward the opposite corners would give the same molecule; for the real tetramers this is not the case. **36** shows that shifting the nitrogens one way locates

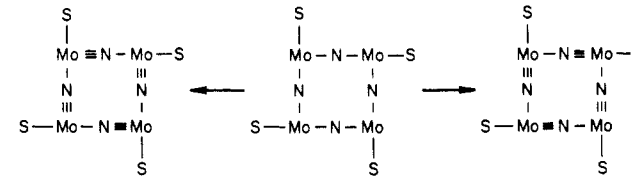

36a **36b** **36c**

short Mo–N bonds trans to the solvent molecules, but moving the nitrogen in the opposite direction places them cis. The Jahn–Teller theorem cannot tell which of the two distortions should be preferred. We carried out some detailed calculations on a less symmetrical model, $[MoNCl_3(OH_2)]_4$.[30] The result we obtain is that structure **36a** is favored over **36c** by 12 kcal/mol. The "D_{4h}" symmetrical structure **36b** is 46 kcal/mol above **36c**. The ordering of **36a** and **36c** is not in agreement with experiment, but the large barrier to nitrogen switching is. We do not know why there is a discrepancy between our model calculations and the real structure, but we are sufficiently confident of the general picture that we anticipate the eventual synthesis of a compound with structure **36a**.

Adding as many as eight more electrons by making each metal d^2 should not change this picture. The distortion would simply

(30) Calculations for $[MoNCl_3(OH_2)]_4$ (C_4 symmetry) were performed with use of bond lengths from the experimental structure of $[MoNCl_3(O(C_4H_9)_2)]_4$ (ref 6a(ii)), except that the O–H distance was taken to be 0.96 Å. Angles about Mo were octahedral angles; the angles about oxygen were tetrahedral. Energies are computed for structures with the experimental Mo–N bond lengths, 1.665 or 2.166 Å.

Table II. Changing the Bridging Atom to a Less Electronegative Element Raises the HOMO, Decreases the HOMO–LUMO Gap, and Increases the Difference in Metal-to-Bridge Bond Lengths

compound	bridge composition	M–bridge dis, Å	M–bridge diff, Å	ref
$[NbF_5]_4$	Nb–F–Nb	2.07, 2.07	0.00	31a
$[NbOCl_3{\cdot}OPCl_3]_4$	Nb–O–Nb	1.74, 2.09	0.35	31b
$[MoNCl_3{\cdot}OPCl_3]_4$	Mo–N–Mo	1.66, 2.15	0.49	6a(iii)
	Mo–C–Mo		predict > 0.49	

empty electrons from b_{1g} into the set of four low-lying levels and stabilize the distorted structure. No tetramers with a d^2 electron count are known, but the Re^{VI} d^1 complex $[ReNCl_3{\cdot}OPCl_3]_4$ shows the expected long and short metal–nitrogen bonds.[6b] As expected from the nature of the second-order Jahn–Teller effect, the square tetramers show a larger difference in metal-to-bridge distances as the bridging atom is made less electronegative. Changing the bridge from fluorine to oxygen and then to nitrogen increases the magnitude of distortion by raising the b_{2g} HOMO and thus decreasing the HOMO–LUMO gap (see Table II). The molecule with a bridging carbon atom has not yet been synthesized, but we would certainly anticipate greater differences in metal-to-bridge bond lengths than any presently known. Lowering the LUMO energy by replacing chloride ligands with σ donors or π acceptors should also enhance the distortion. To data, nitrides having this square geometry have been prepared only with chloride or dithiophosphate ligands.

This brings us to a serious discrepancy between our theoretical framework and experimental results. The compound $[MoN(S_2P(OR)_2)_2]_4$ is observed to have all metal nitrogen bond lengths equal.

Although we calculate a smaller distortion for $[MoN(S_2P(OR)_2)_2]_4$ than for $[MoNCl_4]_4$, we would predict the distortion where none occurs.[6c] Perhaps this is due to the extended Hückel method's well-known failure to reproduce experimental bond lengths accurately. We also understand, however, that the nitrogen b_{2g} orbital becomes mixed up among several sulfur lone pair orbitals of the same symmetry. The consequence is to dilute this orbital's power to stabilize a distortion by decreasing the overlap between the empty metal b_{1g} and the filled b_{2g} orbitals.

Nevertheless, the structure of the molecule remains an anomaly, both by comparison with other nitride tetramer structures, and in relation to our theoretical results. We would urge a careful crystallographic exploration of the structures of some more d^1 dithiophosphate tetramers or related complexes.

The orbital energy level diagram we calculate for $[MoN(S_2P(OR)_2)_2]_4$ shows the five low-lying π^* levels evident in Figure 12. That figure should then give a clue to the nature of the ferromagnetic coupling in $[MoN(S_2P(OR)_2)_2]_4$. The four extra d electrons in this d^1 compound must occupy two or more of the b_{1g}, $2e_g$, b_{1u}, or a_{2u} levels. This concides with the considerations of Noble et al., who attribute the ferromagnetism either to superexchange along the edge of the squre or to direct exchange across the square's diagonals.[6c] For the tetramer with all metal–nitrogen bonds equal, the superexchange mechanism is unlikely because none of the five lowest π^* orbitals contains any appreciable nitrogen component. The nature of the b_{1u} orbital suggests instead direct exchange across the diagonals of the square.

The reader has probably recognized that the bond localization problem considered here for the nitride tetramers resembles the bond alternation found in cyclooctatetraene. Likewise, the polymeric nitrides find a structural and electronic analogue in polyacetylene. We plan to compare these and other nitride compounds with their polyene analogues in a subsequent paper.

Other Polymers

Another way to arrange vertex sharing octahedra cis to one another, alternative to the tetramers, is depicted in **37**. The alternative shown, it should be noted, is one in which the Mo–N skeleton is in a single plane. Still more complicated nonplanar chains may be thought up. Zig-zag chains of type **37** are, to our knowledge, unknown, but the structure can be considered an

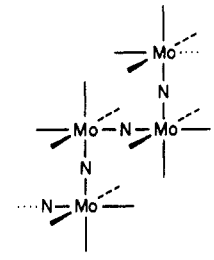

37

idealized version of the VF_5 structure adopted by a number of fluorides and oxyfluorides.[32] The 180° bond angle at the nitrogen is another simplification since angles at the fluoride bridges in VF_5 are closer to 150°. The relevant tetramer orbitals are compared with this polymer's band structure in Figure 13. The tetramer's HOMO and the top of the polymer's valence band appear at the same energy and have the same composition. Similarly, the tetramer's metal-based LUMO marks the bottom of the polymer's conduction band. The three other tetramer π orbitals situated in the molecular plane serve to locate polymer orbitals of similar composition at $k = 0$ and 0.5. As expected, introducing unequal metal–nitrogen bond lengths splits the valence and conduction bands leading to a stabilized second-order Jahn–Teller distorted structure. The transition-metal fluorides which adopt the related VF_5 structure show only tiny bond length alternation.[33]

Perovskites

We will now examine distortions in early transition-metal perovskites, emphasizing their similarity with systems already discussed. The distortions exhibited by the TiO_3^{2-} framework in $BaTiO_3$ are instructive examples which illustrate the general nature of distortions in perovskites involving bond length asymmetries in M–O–M units. (We distinguish these cases from those in which distortions involve mainly M–O–M angle bending.) In **38** we illustrate the distortions of the TiO_3^{2-} framework found in the tetragonal (5 °C $\leq T \leq$ 120 °C), orthorhombic (−80 °C $\leq T \leq$ 5 °C), and rhombohedral ($T \leq$ −80 °C) phases of $BaTiO_3$;[3a,b,f] the structure is cubic above 120 °C up to 1460 °C. The structural relationship between the tetragonal phase and the distorted ML_4X chains is obvious, and a claim that the electronic driving force

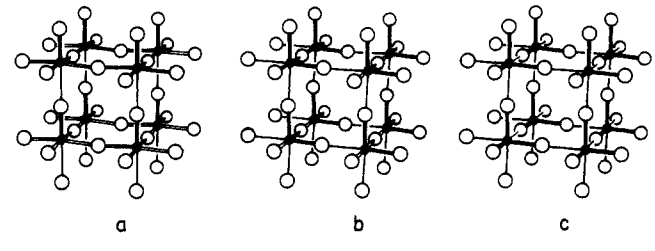

38

for this distortion is similar should hold little surprise. The situation is less clear for the orthorhombic and rhombohedral cases; in the former instance the Ti has moved toward an edge of the surrounding octahedron of oxides yielding two short and two long

(31) (a) Edwards, A. J. *J. Chem. Soc.* **1964**, 3714. (b) Münninghoff, G.; Hellner, E.; El Essawi, M.; Dehnicke, K. *Z. Kristallogr.* **1978**, *147*, 231.

(32) (a) Edwards, A. J. *Adv. Inorg. Chem. Radiochem.* **1983**, *27*, 83. (b) Edwards, A. J.; Jones, G. R. *J. Chem. Soc. A* **1969**, 1651. (c) Edwards, A. J. *Proc. Chem. Soc.* **1963**, 205. (d) Edwards, A. J.; Hugill, D.; Peacock, R. D. *Nature (London)* **1963**, *200*, 672. (e) Edwards, A. J.; Jones, G. R.; Steventon, B. R. *J. Chem. Soc., Chem. Commun.* **1967**, 462. (f) Edwards, A. J.; Steventon, B. R. *J. Chem. Soc. A* **1968**, 2503. (g) Edwards, A. J.; Jones, G. R. *J. Chem. Soc. A* **1968**, 2511.

(33) In VF_5, for example, V–F_{bridge} distances are 1.93 and 2.00 Å.[32b]

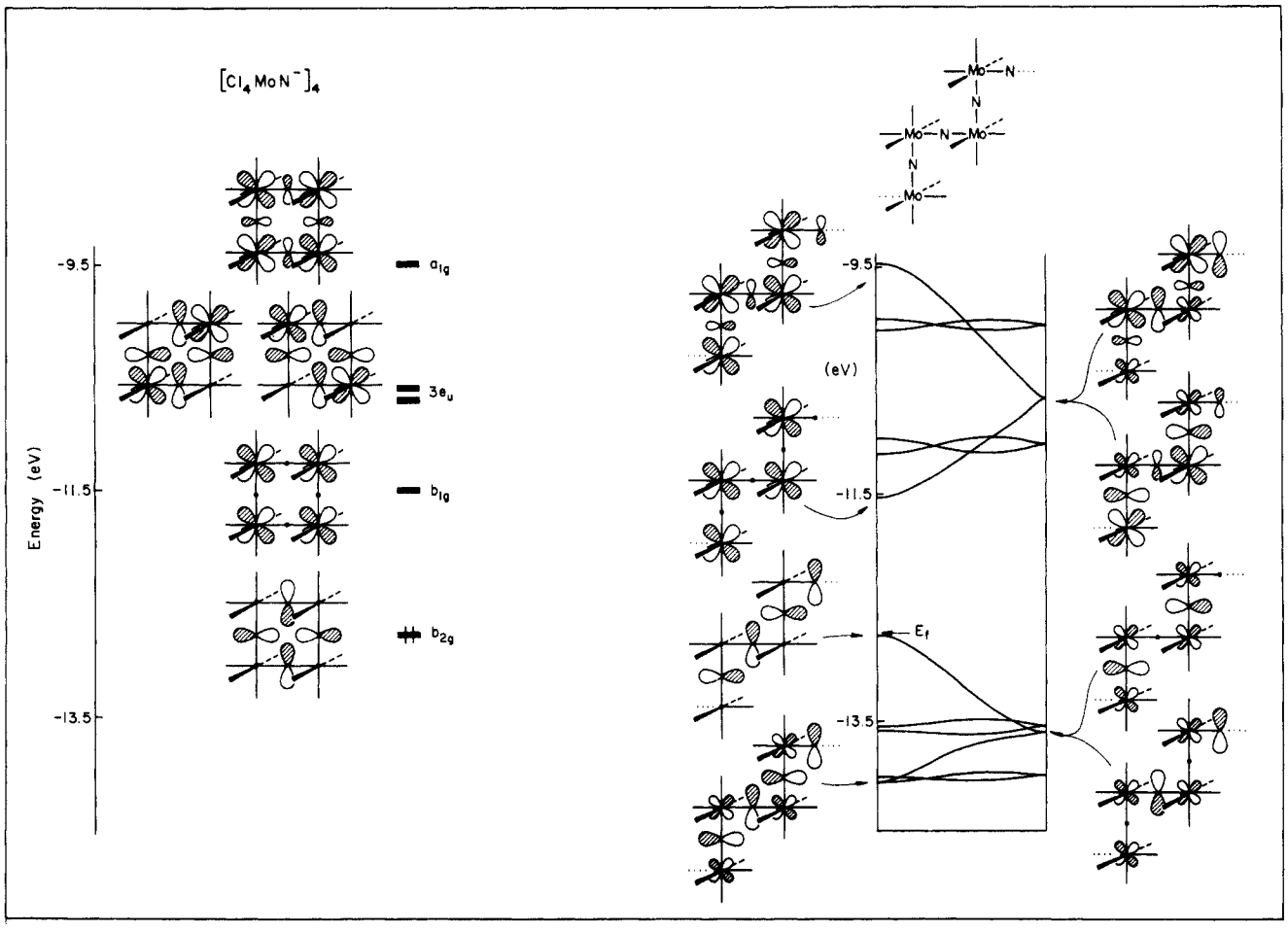

Figure 13. Tetramer π orbitals situated in the molecular plane (a) serve to locate the corresponding orbitals of the cis octahedral polymer $MoNCl_4^-$ at $k = 0$ and 0.5 (b).

Ti–O linkages, and in the latter structure the Ti has moved toward a face of the oxide octahedron to give three short and three long Ti–O distances. Why should these structures have comparable energies? $KNbO_3$[3h] and WO_3[3c-e] exhibit a similar variety of polymorphs but Na_xWO_3 ($x \simeq 1$) and ReO_3 have cubic MO_3 frameworks.

It is convenient to state the results of our calculations on a NbO_3^{n-} ($n \geq 1$) net and then backtrack to provide some interpretation. First, we find that for a d^0 system, the cubic system is unstable with respect to any of the three distortions illustrated in **38** to an approximately equal extent. Second, as the d electron concentration is increased from zero the cubic structure becomes increasingly stabilized. Figure 14 illustrates this effect: the two curves shown illustrate the trend in the energy difference between the cubic and tetragonal structures with varying degrees of distortion assumed. Where the curves are above the base line the symmetrical (cubic) structure is favored. Curves for the orthorhombic and rhombohedral distortions were also calculated and were very similar to that shown for the tetragonal case. Note that the asymmetric to symmetric "crossover" occurs near the d^1 concentration. Experimentally, the crossover seems to occur for lower d electron concentrations; e.g., ReO_3 is cubic, a high pressure phase with composition $K_{0.92}MoO_3$ is known,[3k] and the pseudocubic phases Na_xWO_3, Li_xWO_3,[3a,b,f] $Ba_{0.5+x/2}NbO_3$,[3i] and $Sr_{0.5+x/2}NbO_3$[3i] have been reported for $x < 1$. This quantitative discrepancy between our theoretical results and experiment is again atttributable to the inadequate "restoring force" provided by the σ-bonding electrons in our calculations. It further buttresses our interpretation of the nature of the extended-Hückel method's shortcomings in application to systems discussed previously (because in the 3-dimensional extended system *both* symmetric and asymmetric structures are already known).

For understanding the M–O π bonding in ReO_3-like nets and distorted variants, we have found a simple Hückel model to be

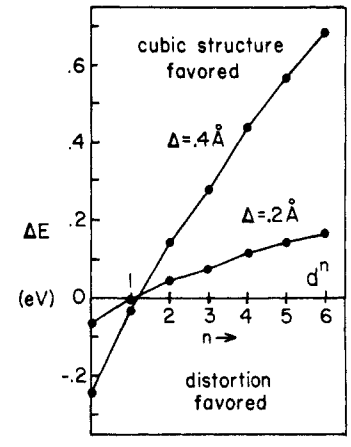

Figure 14. Energetics of the tetragonal distortion of a model NbO_3 net as a function of the formal d electron count. The two different lines correspond to greater ($\Delta = 0.4$ Å) and lesser ($\Delta = 0.2$ Å) bond length differences between the long and short M–O bonds parallel to the tetragonal axis.

very instructive. An important first step in tackling the π-bonding problem in the 3-dimensional ReO_3 structure is the recognition that it is easily reduced to a two-dimensional problem. This can be seen by inspection of **39** where we show Re d_π and O p_π orbitals which project into the xz and zy interpenetrating planes. Interactions between orbitals associated with parallel planes (e.g., xy–xy) will be very small due to the large separation (~4 Å) between planes. Furthermore, interactions between orbitals lying in intersecting planes (e.g., xy–xz) will be small because the d_π orbitals in a given plane present a sigma overlap to adjacent oxygens lying on a normal to the plane in which that metal center resides. Thus, to an excellent approximation, we may restrict our

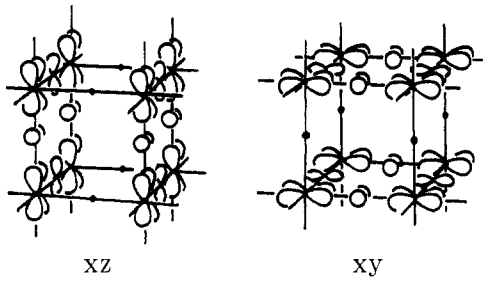

39

attention in solving π-electron problems to a single plane (see **40**).

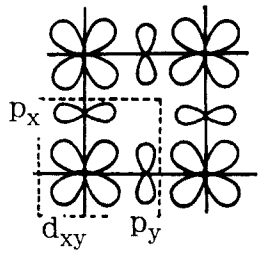

40

The distortions of **38** have a different effect on the interpenetrating planes of the ReO_3 net. The tetragonal distortion perturbs the *xz* and *yz* π systems but leaves the *xy* system virtually unchanged since none of the bonds in the *xy* planes are stretched or shortened. Assuming the distortion is small we may consider the perturbation of the *xz* and *yz* systems as depicted in **41a**—the short bonds' resonance integral increases as that for the long bonds decreases. The orthorhombic distortion perturbs one of the π

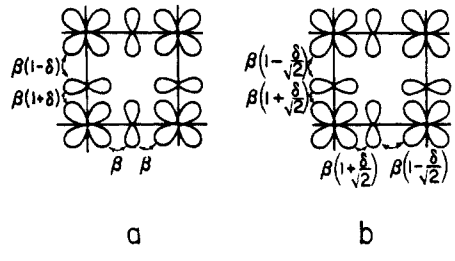

41

systems (say *xz*) as illustrated in **41b** while the *xy* and *yz* systems are perturbed in the manner of **41a** (except that δ must be replaced by $\delta/\sqrt{2}$). The rhombohedral distortion perturbs all the systems as in **41b** (except that $\delta/\sqrt{2}$ should be replaced by $\delta/\sqrt{3}$). The factors of $1/\sqrt{2}$ and $1/\sqrt{3}$ arise from our desire to compare distorted structures in which the effective displacement of the metal atoms from the centers of the surrounding oxide octahedra is the same in each instance.

Each of the mathematical problems posed by **40** and **41** have analytical (if clumsy) solutions.[34] But the essential features of the problem can be understood without getting into the details. The unit cell in every case consists of one d orbital and two oxide p orbitals. For any given $\vec{k}$, the phase relationship between all the d orbitals throughout the 2-dimensional system is *fixed* (by Bloch's theorem and the translation symmetry it implies). There must a linear combination of the Bloch sum built from the *two* p orbitals which is exactly orthogonal to the *single* Bloch sum built from the d orbitals. Therefore, for *every* $\vec{k}$ there will be one crystal orbital which has purely oxide character and is nonbonding (this implies on our neglect of next-nearest-neighbor O–O interactions). This special situation yields a perfectly flat band that has been called "superdegenerate" by one of us and is more fully described

(34) Hughbanks, T. *J. Am. Chem. Soc.*, submitted for publication.

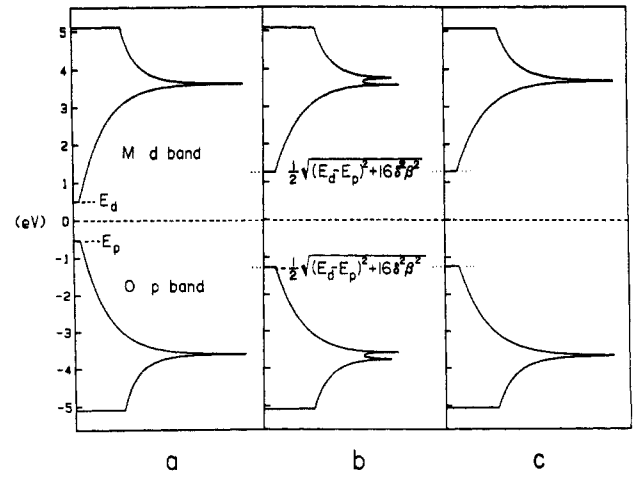

Figure 15. DOS curves for the M–O π bands are depicted: (a) the undistorted case, (b) the *xz* and *yz* bands for the tetragonal distorted case (**41a**), and (c) *xz* bands for the orthorhombic distortion (**41b**). The flat nonbonding oxide p band is not shown for any case. The curves shown are for $E_d - E_p = 1.0$ eV, $\beta = 1.8$ eV, $\delta = 0.33$.

elsewhere.[34] Since the nonbonding band occurs unchanged for all cases **40**, **41a**, and **41b**, we will not consider it further. The density of states reduces to just two significant bands in every case—Figure 15 gives a diagram of the DOS for distorted and undistorted cases.[35]

The effect of distortion on the DOS is clear: the oxide p and metal d bands repel each other and the gap between them widens. Notably, the distortions **41a** and **41b** open gaps of equal magnitude and the gain in energy afforded by stabilization of the low-lying oxide p band is virtually identical for the two classes. The origin of the gap widening is completely analogous to the situation found for the ML_3X and ML_4X chains and the ML_4X tetramer. At the top of the oxide band is a nonbonding combination of d orbitals—each corresponding to $\vec{k} = 0$. As illustrated for case **41b** in **42** the symmetry breaking introduced by the distortion allows these nonbonding orbitals to mix. The magnitude of the energy shift can be estimated by perturbation theory to be $4\delta^2\beta^2/(E_d - E_p)$ and is a second-order correction. (The exact expression in Figure 15 reduced to this for a small δ.) Once again we have a second-order Jahn–Teller distortion, and for the same reason: the second-order mixing of the M d_π and O p_π level drives the distortion.

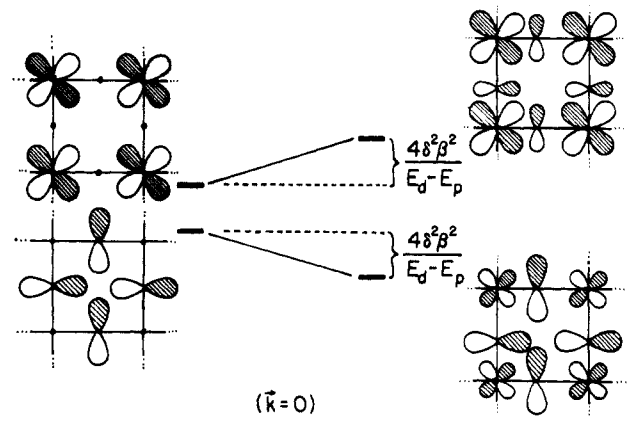

42

There is one feature of our results for MO_3 systems which is quite different from those for ML_4X chains: for the chain com-

(35) The simple model outlined should be compared with previous detailed calculations: (a) For ReO_3 see: Mattheiss, L. F. *Phys. Rev.* **1969**, *181*, 987. (b) Other perovskites: Mattheiss, L. F. *Phys. Rev. B.: Condens. Matter* **1972**, *6*, 4718. (c) Our treatment should be compared with that of ref 15a.

pounds d^0, d^1, and d^2 systems usually behave similarly, but the 3-dimensional framework is such that any d electron concentration above d^0 works in favor of the cubic structure. This result may appear to be anomalous in view of the close structural similarity between the distortions illustrated for $ReNCl_4$ in **3**, or $VOPO_4$ in **4**, and tetragonal $BaTiO_3$ in **38a**. The origin of this apparent discrepancy is made clear when we think about "where d electrons must go" when they are added to the d^0 systems. In both the ML_4X chains and the tetragonal MO_3 systems the *xy* orbitals are unaffected by the MX bond alternation along the *z* axis. However, in the chain compounds, the *xy* orbitals lie low in energy in the absence of strong π donors as ligands. This leaves this orbital available to accommodate the first two d electrons added to the d^0 system. The *xy* orbitals in the perovskites *are* involved in π bonding with the surrounding oxides and the *xy* band has a relatively large width. In a reduced perovskite (d^n with $n > 0$) subject to a tetragonal distortion, electrons will be effective transferred from the {*xz*, *yz*} manifold to the *xy* manifold—"on top" of the already occupied *xy* levels. The situation for a d^1 case is depicted in **43**: for a cubic structure, the three t_{2g} orbitals will

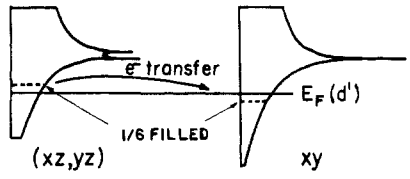

43

each be $^1/_6$th full; if a distortion occurs the {*xz*, *yz*} bands will be pushed up (as the corresponding oxide π bands are stabilized) and some electron density will flow into *xy* levels barely lower in energy. The energy recouped by electron transfer falls well short of compensating for the destabilization of the {*xz*, *yz*} manifold. It is important that the crystal orbital energy of the t_{2g}-type d levels rises sharply with d electron concentration at the bottom of the band. This quickly makes the *xy* orbitals energetically inaccessible as the count rises from zero.

Our treatment is not faultless. Perhaps the most minor drawback is our inability to rank various distorted structural alternatives for d^0 in order of increasing energy. For example, our tetragonal, orthorhombic, and rhombohedral structures were all within a few kcal/mol in energy—and the differences found could easily be inverted by different assumptions in the structural parameters used in the calculations. In view of the remarkable polymorphism exhibited by compounds such as $KNbO_3$,[3h] $BaTiO_3$,[3a,b,g] and WO_3,[3a] it must be that the (internal) energy differences separating distorted alternatives are indeed small. A more serious limitation of our results is lack of discrimination between various d^0 systems and the fact that a few such systems (such as $SrTiO_3$)[3a,b] are *not* subject to bond alternation distortions. It would appear that oxide systems are indeed closer to the point of crossover between symmetric and asymmetric behavior than our numerical results have shown. The inadequacy of extended-Hückel calculations in modelling the "classical" restoring force inhibiting second-order Jahn–Teller distortions has to be borne in mind for the 3-dimensional networks as well as for chains and tetramers. Finally, we should note that the range of systems to which our treatment is directly applicable is limited. For AMO_3 systems in which A is a vacancy or an alkali or alkaline earth element our assumption that A has no role other than that of an electron donor will often be justified. Even in those cases, the effective radius of the A cation cannot be ignored (e.g., Li^+) causes M–O–M bending in order to accommodate the small cation). For cations such as Pb^{2+} or lanthanides, the role of A–O orbital interactions will need to be more carefully considered.

Table III. Parameters Used in the Extended Hückel Calculations

orbital		H_{ii}, eV	ζ_1	ζ_2	C_1[a]	C_2
W	5d	−10.40	4.98	2.07	0.6683	0.5422
	6s	−8.26	2.34			
	6p	−5.17	2.31			
Mo	4d	−12.3	4.54	1.901	0.5899	0.5899
	5s	−9.66	1.956			
	5p	−6.36	1.901			
Nb	4d	−12.1	4.08	1.64	0.6401	0.5516
	5s	−10.1	1.89			
	5p	−6.86	1.85			
Cl	3s	−30.00	2.033			
	3p	−15.00	2.033			
O	2s	−32.30	2.275			
	2p	−14.80	2.275			
N	2s	−26.00	1.95			
	2p	−13.40	1.95			
H	1s	−13.60	1.30			

[a] Exponents and coefficients used in double-ζ expansion of d orbitals.

Conclusions

The essential common features in the electronic structure of all the molecular and extended systems we have discussed are the bridging atom based HOMO (valence band) and the metal centered LUMO (conduction band). These levels are mixed and pushed apart by vibrations of the appropriate symmetry to enable otherwise nonbonding orbitals to form bonding and antibonding combinations. The stabilization of the filled bonding orbitals drives the distortion. Consistent with its characterization as a second-order Jahn–Teller distortion, bond alternation decreases with the increasing electronegativity of the bridging ligand and concomitant increase in the HOMO–LUMO gap (valence-conduction band gap). For d^n perovskites ($n > 0$), the stereochemical role of the d electrons in highlighted. Filling the conduction band swiftly negates the stabilization that distortion confers upon oxide centered p_π bands. This supports our contention that symmetrically bridged ML_n polymers should be feasible if the d electron count can be made high enough to partially fill the d_π bands.

Bond alternation in ML_nX chains should be even more pronounced in carbido-bridged analogues to the nitrides discussed. Because the valence–conduction band gap would be narrowed, the use of π-acceptor ligands should achieve the same end.

Acknowledgment. T. A. Albright thanks the Robert A. Welch Foundation for partial support along with the Alfred P. Sloan and Camille and Henry Dreyfus Foundations for fellowships. M.-H. Whangbo is grateful to the Camille and Henry Dreyfus Foundation for a Teacher-Scholar Award (1980–1985). The work at Cornell was supported by the National Science Foundation through Research Grant DMR 8217277 AO2 to the Materials Science Center. Work at the University of Chicago was funded by Dow Chemical and the donors of the Petroleum Research Fund, administered by the American Chemical Society.

Appendix

Extended Hückel calculations[9] were performed with use of metal parameters from previous calculations[36] and listed in table III. The geometry for $[WN(OH)_3]_x$ was taken from the experimental structure of the *tert*-butyl derivative[11b] except that an O–H distance of 0.96 Å and W–O–H angles of 136.6° were used. Bond lengths for calculations involving $MoNCl_4^-$ were taken from the experimental structure for $[MoNCl_3{\cdot}O(C_4H_9)_2]_4$.[6a(ii)]

(36) (a) Tatsumi, K.; Hoffmann, R. *Inorg. Chem.* **1980**, *19*, 2656. (b) Hoffman, D. M.; Hoffmann, R.; Fisel, C. R. *J. Am. Chem. Soc.* **1982**, *104*, 3858. (c) Whangbo, M.-H.; Foshee, M. J. *Inorg. Chem.* **1981**, *20*, 113.